Geophysical Journal International

Geophys. J. Int. (2010) **181,** 1214–1246 doi: 10.1111/j.1365-246X.2010.04591.x

Oroclinal bending, distributed thrust and strike-slip faulting, and the accommodation of Arabia–Eurasia convergence in NE Iran since the Oligocene

James Hollingsworth,[1] Morteza Fattahi,[2,3] Richard Walker,[4] Morteza Talebian,[5] Abbas Bahroudi,[6] Mohammad Javad Bolourchi,[5] James Jackson[7] and Alex Copley[1]

[1]*Division of GPS, California Institute of Technology, MC 100–23, Pasadena, CA* 91125, *USA. E-mail: james@gps.caltech.edu*
[2]*Institute of Geophysics, University of Tehran, Kargar Shomali, Tehran,* PO Box 14155–6466, *Iran*
[3]*School of Geography, University of Oxford, South Parks Road, Oxford* OX1 3QY, *UK*
[4]*COMET-NCEO & Department of Earth Sciences, University of Oxford, Parks Road, Oxford* OX1 3PR, *UK*
[5]*Geological Survey of Iran, Azadi Sq., Meraj Avenue,* PO Box 13185–1494, *Tehran, Iran*
[6]*Exploration Department, University of Tehran, Tehran,* PO Box 11365–4563, *Iran*
[7]*COMET-NCEO & Bullard Laboratories, University of Cambridge, Madingley Road, Cambridge* CB3 0EZ, *UK*

Accepted 2010 March 7. Received 2010 February 2; in original form 2009 January 24

SUMMARY

Regional shortening is accommodated across NE Iran in response to the collision of Arabia with Eurasia. We examine how N–S shortening is achieved on major thrust systems bounding the eastern branch of the Alborz (east of 57°E), Sabzevar and Kuh-e-Sorkh mountain ranges, which lie south of the Kopeh Dagh mountains in NE Iran. Although these ranges have experienced relatively few large earthquakes over the last 50 yr, they have been subject to a number of devastating historical events at Neyshabur, Esfarayen and Sabzevar. A significant change in the tectonics of the eastern Alborz occurs directly south of the Central Kopeh Dagh, near 57°E. To the east, shortening occurs on major thrust faults which bound the southern margin of the range, resulting in significant crustal thickening, and forming peaks up to 3000 m high. Active shortening dies out eastward into Afghanistan, which is thought to belong to stable Eurasia. The rate of shortening across thrust faults bounding the south side of the eastern Alborz north of Neyshabur is determined using optically stimulated luminescence dating of displaced river deposits, and is likely to be 0.4–1.7 mm yr^{-1}. Shortening across the Sabzevar range 150 km west of Neyshabur has previously been determined at 0.4–0.6 mm yr^{-1}, although reassessment of the rate here suggests it may be as high as 1 mm yr^{-1}. Migration of thrust faulting into foreland basins is common across NE Iran, especially in the Esfarayen region near 57°E, where the northward deflection of the East Alborz range reaches a maximum of 200 ± 20 km (from its presumed linear E–W strike at the beginning of the Oligocene). West of 57°E, the tectonics of the Alborz are affected by the westward motion of the South Caspian region, which results in the partitioning of shortening onto separate thrust and left-lateral strike-slip faults north and south of the range. At the longitude of 59°E, published GPS velocities indicate that 50 per cent of the overall shortening across NE Iran is accommodated in the Kopeh Dagh. The remaining 50 per cent regional shortening must therefore be accommodated south of the Kopeh Dagh, in the eastern Alborz and Kuh-e-Sorkh ranges. Assuming present day rates of slip and the fault kinematics are representative of the Late Cenozoic deformation in NE Iran, the total 200 ± 20 km N–S shortening across the eastern Alborz and Kopeh Dagh mountains since the beginning of uplift of the Kopeh Dagh basin would be accommodated in 30 ± 8 Ma. Although this extrapolation may be inappropriate over such a long timescale, the age is nevertheless consistent with geological estimates of post Early-to-Middle Oligocene (<30 Ma) for the onset of Kopeh Dagh uplift.

Key words: Geomorphology; Seismicity and tectonics; Continental neotectonics; Tectonics and landscape evolution; Asia.

1 INTRODUCTION

Iran occupies a place of special importance in the study of active continental collisions. It is situated between the Eurasian and Arabian plates, which converge at about 25 mm yr^{-1}, and virtually the entire active collision zone is contained within the geographical and political borders of the country (Fig. 1a). The orogen is therefore uniquely compact and accessible, and active geomorphological features are generally well exposed and preserved in the desert or arid climate. Within Iran, many features of continental tectonics that are of generic importance are well known, such as partitioning of oblique motions onto parallel strike-slip and thrust faults (Talebian & Jackson 2004; Vernant *et al.* 2004a), block rotations about vertical axes (Walker & Jackson 2004; Copley & Jackson 2006), and the concentration of deformation around the edges of rigid blocks within the collision zone (Jackson *et al.* 2002; Masson *et al.* 2005; Reilinger *et al.* 2006). Recent syntheses of the active tectonic motions in various parts of Iran (e.g. Walker & Jackson 2004; Regard *et al.* 2005; Hessami *et al.* 2006; Meyer *et al.* 2006; Ritz *et al.* 2006; Walpersdorf *et al.* 2006) all emphasize the three-dimensionality of continental tectonics, first highlighted by McKenzie (1972) and Molnar & Tapponnier (1975).

Within Iran, the NE part of the country, which is the subject of this paper, is also special. Seismicity, GPS and active geomorphology all reveal an abrupt edge to the collision zone, trending N–S along the eastern border between Iran and Afghanistan, and trending NW–SE along the northern border with Turkmenistan (Fig. 1). The N to NNE convergence between Arabia and Eurasia requires Iran to be compressed into this NE corner, and this simple geometry dominates the pattern of strains within the country (Jackson *et al.* 1995; Masson *et al.* 2005). Along its eastern border, the north-south right-lateral shear between Iran and Afghanistan is accommodated by N–S right-lateral strike-slip faults in the southern part, but the faulting then changes to E–W left-lateral faults on the north side of the aseismic Lut block, which can only accommodate the shear by rotating clockwise (Walker & Jackson 2004), see Fig. 1(b). Further north still, that shear must end by shortening against the edge of the Turkmen shield in the high mountains of the Kopeh Dagh and its adjacent ranges. Yet some of this shortening is also achieved by a westward movement of the aseismic South Caspian Basin relative to both Iran and Eurasia, which is, in turn, related to an along-strike extension of the Kopeh Dagh mountains (Hollingsworth *et al.* 2006, 2008).

The subject of this paper is the region immediately south of the Kopeh Dagh mountains which run along the Turkmenistan border (Fig. 1c). This is a crucial region that must somehow accommodate (1) the north–south transition from right-lateral shear and clockwise rotation along the Afghan border to shortening against Turkmenistan and (2) the transition from shortening in the east, to lateral 'expulsion' of the South Caspian Basin on obliquely convergent and partitioned strike-slip systems to the west (transpression). Spatial transitions of this sort are probably common in continental collisions, but rarely as active or as well exposed as in this case: the region is therefore of much more than local significance. There is a wealth of data from earthquake focal mechanisms, observations of faulting in the field and some GPS measurements (which are likely to become much more abundant in the future). Individually these data sets provide only limited information on the active tectonics of an area. However, when used together, they allow the first order features of the deformation to be identified, thereby providing a far more robust and coherent picture of the regional kinematics. The aim of this paper is to summarize in one place, so that the kinematics of this whole important transitional region is visible together, what is known of the active faulting and how it accommodates motions within and across the zone. Once a regional kinematic model has been established for this region, it will provide a framework for future more detailed studies, thereby further refining the model.

Before this study the location of active faults in this region was virtually unknown and not reported in the literature. Therefore, in Sections 3–7 we describe in detail various fault systems throughout the region, before discussing their role in accommodating Arabia–Eurasia shortening in Section 8. We make use of field and remote-sensing observations, geomorphological information about fault slip rates, and accounts of historical earthquakes, which highlight both the activity on structures and also the significant risk to several densely populated modern cities that have been destroyed, some of them several times, in the past.

2 TECTONIC AND GEOLOGICAL BACKGROUND

2.1 Regional tectonics and geographic setting

The collision of the Arabian plate with Eurasia is accommodated by shortening across the Iran region. Recent GPS measurements (Sella *et al.* 2002; McClusky *et al.* 2003; Vernant *et al.* 2004b; Masson *et al.* 2007) indicate that Arabia moves northward, with respect to Eurasia, at ∼23 mm yr^{-1} at the longitude of the NE Iran (Fig. 1a). Both the northward decrease in GPS velocities, and the large number of earthquakes across Iran indicates that much of the deformation is concentrated in the Zagros, Alborz, Talysh and Kopeh Dagh mountain ranges, by subduction beneath the central Caspian sea (Apsheron-Balkan sill), and the Makran, and on N–S right-lateral fault systems in East Iran—see Fig. 1(b). These areas surround the relatively aseismic Central Iran (CI), South Caspian (SC) and Lut desert (L) regions, which contribute little to the regional shortening and probably behave as relatively rigid blocks (Jackson & McKenzie 1984). West of 57°E, the Zagros accommodates about half of the northward motion of Arabia (e.g. Tatar *et al.* 2002), with the Alborz and central Caspian sea taking up the rest further north. East of 57°E, about half of the northward motion of Arabia is accommodated by subduction beneath the Makran, with the remainder accommodated on various intracontinental mountain belts in East and NE Iran. The low velocity of station ZABO, which lies east of the Lut block, indicates Afghanistan is part of stable Eurasia, and no extrusion of continental material occurs to the east. Shortening north of the Zagros requires N–S right-lateral strike-slip faulting between Central Iran and stable Afghanistan. This is observed in the N–S right-lateral fault systems either side of the Lut desert, in east Iran (e.g. Walker & Jackson 2002, 2004). Therefore, shortening in Iran is accommodated primarily by partitioning onto separate thrust and strike-slip systems. The relatively complicated pattern of faulting is probably due to the influence of pre-existing structural weaknesses, which have been reactivated in the Late Cenozoic (Allen *et al.* 2006).

Detailed GPS studies have been undertaken in the Zagros and central Alborz (Tatar *et al.* 2002; Vernant *et al.* 2004a), which allow a better understanding of their role in accommodating Arabia–Eurasia convergence. Although similar studies have not been undertaken in NE Iran, where shortening is both slower and more distributed, GPS velocities from coarsely-spaced stations at KASH, SHIR, MSHN and YAZT allow a general assessment of deformation in NE Iran (Fig. 1c). These show 6 mm yr^{-1} N–S shortening between Kashmar

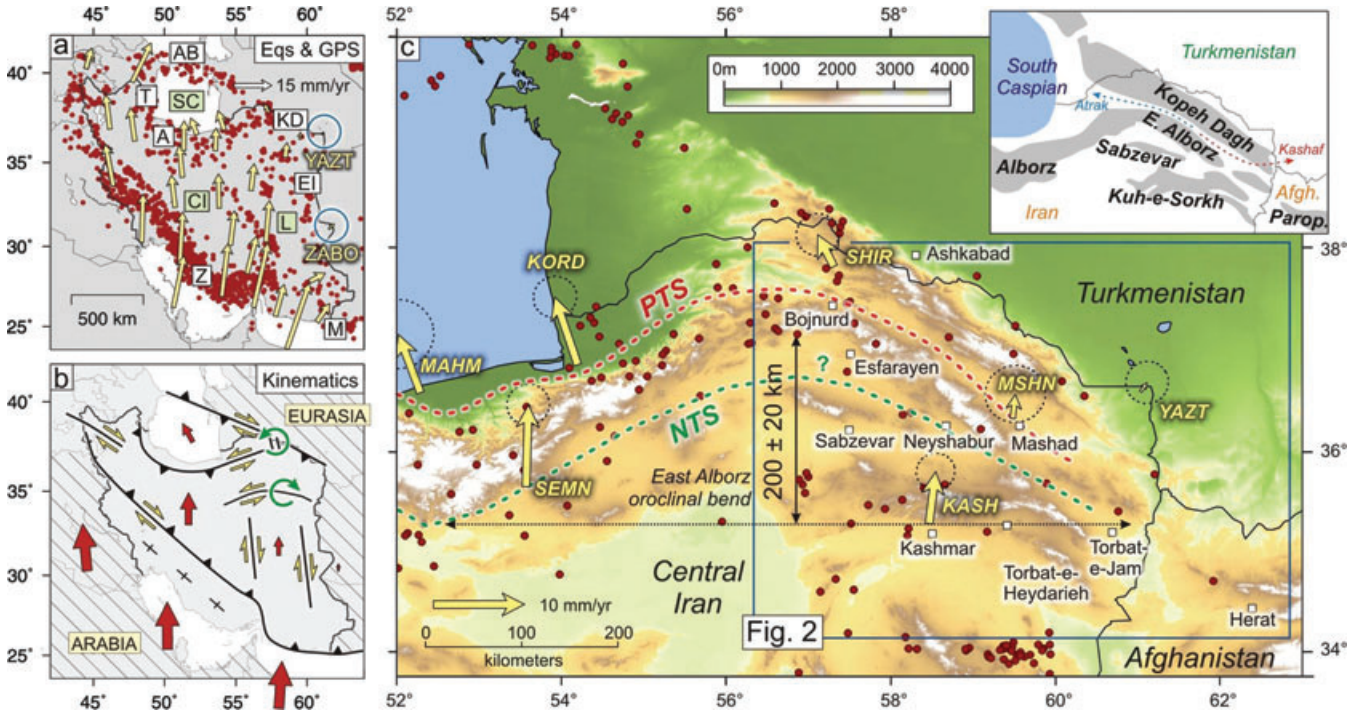

Figure 1. (a) GPS velocities relative to Eurasia record 25 mm yr^{-1} N–S shortening between Arabia–Eurasia, which is accommodated throughout Iran (Masson *et al.* 2007). Blue circles highlight the low velocities of GPS stations YAZT and ZABO, which lie along the north and eastern border of Iran. Red dots show locations of earthquake epicentres ($M_w \geq 5.1$) across Iran during the period 1964–2004 (Engdahl *et al.* 1998, 2006). Earthquakes are concentrated in the Zagros (Z), Talysh (T), Alborz (A) and Kopeh Dagh (KD) mountain belts, the strike-slip fault systems of East Iran (EI), and the Apsheron-Balkan (AB) and Makran (M) subduction zones, which surround the relatively aseismic Central Iran (CI), Lut desert (L) and South Caspian (SC) blocks. (b) Schematic summary map showing the present day kinematics of Iran. Red arrows, indicating motions relative to Eurasia, show approximately how N–S shortening is accommodated across the region. Black lines show the nature of deformation across major fault zones. Yellow arrows indicate the sense of slip for strike-slip faults. Green arrows indicate the direction of vertical axis block rotations, which play an important role in accommodating Arabia–Eurasia convergence across E and NE Iran (see Walker & Jackson 2004). (c) Summary topographic map of the NE Iran region. Major cities discussed in the text are shown. Dotted red line shows the Palaeotethys suture; dotted green line shows the Neotethys suture, which is less well documented for NE Iran (Alavi 1996). Yellow arrows show GPS velocities for NE Iran, with 95 per cent error ellipses (Masson *et al.* 2007). Red dots show locations of recent (mb > 4.8) earthquakes in NE Iran, from Engdahl *et al.* (2006). Turkmenistan and Afghanistan are relatively aseismic, and form the southern margin of Eurasia. The East Alborz has been deflected to the north by 200 ± 20 km at the longitude of 57°E. For clarity, the various mountain ranges of NE Iran (shown in grey) are labelled on the inset map. The Paropamisus mountains of NW Afghanistan (Afgh.) are labelled Parop. Blue and red lines show the Atrak and Kashaf rivers, which flow along the Palaeotethys suture zone and separates the Kopeh Dagh from the Alborz.

(KASH), south of the Kuh-e-Sorkh, and the stable Turkmenistan (Turan) platform (YAZT), north of the Kopeh Dagh (Eurasian plate). This motion is accommodated across subparallel mountain ranges in NE Iran: from north to south, these are the Kopeh Dagh, East Alborz, Sabzevar (Siah Kuh or Joghatay) and Kuh-e-Sorkh ranges (Fig. 1c inset).

The northern-most range is the NW-trending Kopeh Dagh, which reaches elevations of 3000 m and forms the northern limit to Arabia–Eurasia deformation in NE Iran. Shortening across the Kopeh Dagh is currently accommodated on range-bounding thrust faults east of 59°E, anticlockwise rotation of right-lateral strike-slip faults between 57–59°E, and westward extrusion of material along thrust and strike-slip faults west of 57°E (for further details on the active tectonics of the Kopeh Dagh, see Tchalenko 1975; Lyberis & Manby 1999; Hollingsworth *et al.* 2006, 2008; Shabanian *et al.* 2009b, and later discussion in Section 8). The Kopeh Dagh are separated to the south from the eastern branch of the Alborz mountains (hereafter referred to as the East Alborz) by the relatively narrow Atrak-Kashaf river valley which follows the Palaeotethys suture (Fig. 1c inset). A syntaxis occurs in the East Alborz range between 52 and 60°E, with essentially the same geology outcropping all along this part of the range (for a summary geological map of the NE Iran region, see Appendix S1), and reaches a maximum northward deflection of ∼200 km (from an assumed original E–W strike) at the longitude of 57°E (Fig. 1c). Southeast of this syntaxis, the East Alborz strike NW–SE and the elevation of the range is comparable with the Kopeh Dagh, reaching 3000 m at the longitude of Neyshabur between 58.5 and 59.5°E (this section of the range is known locally as the Binalud mountains, e.g. Alavi 1992), before dying out to the east near the Afghanistan border. Southwest of the syntaxis at 57°E, the East Alborz strike NE-SW and decrease in elevation, with peaks reaching 2000 m near 56°E, before increasing again to 4000 m in the Central Alborz. The Sabzevar mountains (also known as the Siah Kuh or Joghatay mountains) lie 80 km south of the East Alborz, and strike ESE for 200 km between 56.5 and 58.5°E (Fig. 1c inset). The Kuh-e-Sorkh mountains lie 80 km south of Sabzevar, and strike E–W for 350 km between 57 and 60.5°E. Both the Sabzevar and Kuh-e-Sorkh mountain ranges reach elevations up to 2800 m high.

2.2 Geology

Due to the importance of the inherited geological structure in NE Iran dictating the pattern of present-day deformation, we briefly

summarize the geological evolution of this region from published studies and our own deductions based on the geological maps of Huber (1977a,b). The geological history of NE Iran involved a period of relative quiescence and stable shelf sedimentation during the Palaeozoic, followed by continental collision during the Mesozoic and Cenozoic, which continues today. Collision started in the Late Triassic and Late Jurassic (Cimmerian Orogeny), when the Central-and-East Iran microplate collided with Eurasia (northern Pangea). The collision resulted in the closure of the Palaeotethys ocean along a suture zone (Palaeotethys Suture Zone; PTS in Fig. 1c) which runs along the north side of the Alborz and follows the Atrak-Kashaf valley in NE Iran (Berberian & King 1981; Şengör 1984; Alavi 1996). During the Cretaceous the Central-and-East Iran block became separated from Eurasia by a newly formed branch of the Neotethys ocean (Stöcklin 1974). During the end of the Cretaceous and early Palaeocene, shortening along the northern margin of Neotethys resulted in the collision of the Central-and-East Iran microplate with Eurasia, marking the onset of the Alpine-Himalayan Orogeny, and the formation of an early Alborz mountain chain (Berberian 1981; Alavi 1996; Guest *et al.* 2006a). During collision the narrow band of Neotethys between Central-and-East Iran and Eurasia was subducted, and ophiolitic material was emplaced across NE Iran south of the Alborz mountains (e.g. the Sabzevar and Kuh-e-Sorkh ophiolites, see Appendix S1). Once Central-and-East Iran was resutured to Eurasia (along the Neotethyan Suture Zone; NTS in Fig. 1c) subduction of Neotethys shifted to the southern margin of Central-and-East Iran.

In NE Iran, the East Alborz consist of unmetamorphosed Palaeozoic and Mesozoic deposits; predominantly Jurassic limestone. An exception occurs in the the Binalud section of the East Alborz (north of Neyshabur) where Jurassic limestones are absent, and Palaeozoic to Jurassic exposures have been metamorphosed. The Binalud provide a window into the older Cimmerian structure of NE Iran, which has been overprinted by later Alpine movements (Alavi 1992). During the Palaeocene, Alborz-derived molasse was deposited in the South Caspian and Kopeh Dagh sedimentary basins, north of the range, which may have resembled the present-day Persian Gulf foreland basin south of the Zagros mountains. During the Eocene (56–34 Ma), widespread volcanism occurred throughout NE Iran and the Alborz (absent in the South Caspian and Kopeh Dagh basins), which is thought to record a period of backarc extension related to the northward subduction along the Zagros suture (Alavi 1996; Vincent *et al.* 2005; Guest *et al.* 2006a; Zanchi *et al.* 2006). Meanwhile, increased uplift and erosion of the Alborz occurred during the Oligocene (34–23 Ma— Afshar-Harb 1979; Berberian & King 1981; Alavi 1996), which is reflected by a pulse in exhumation at 32 Ma recorded by apatite-fission track data from the west and central Alborz (Rezaeian 2009). The early Oligocene probably corresponds to the initial stages of Arabia–Eurasia collision, based on the regional change from extension to convergence, unconformable deposition of terrestrial sediments across the Alborz, and decelerated volcanism across the region (Vincent *et al.* 2005), although a recent compilation of geological data by Allen & Armstrong (2008) suggests a slightly later onset at ∼35 Ma (Late Eocene). The onset of collision may have been in response to the initial opening of the Red Sea between 20 and 30 Ma (Hempton 1987).

Uplift of the Kopeh Dagh basin, north of the East Alborz, occurred sometime after the early-to-middle Oligocene (post 30 Ma, Berberian & King 1981; Golonka 2004), with an unconformable change from marine (Eocene Khangiran Formation) to terrestrial (Miocene? continental red beds; similar to the post-20 Ma Upper Red Formation of the central Alborz) sedimentation occurring during the Oligocene–Early Miocene (34–20 Ma). As the Kopeh Dagh became uplifted in NE Iran, the South Caspian, north of the west and central Alborz, remained a sedimentary basin. Therefore, shortening was focused in the west and central Alborz (where the range is both wider and higher than the East Alborz) south of the rigid South Caspian backstop, while shortening in NE Iran migrated north (distributed across both the Alborz and Kopeh Dagh) as the Kopeh Dagh basin was uplifted. Rezanov (1959) recognized a gradual northward migration of the Kopeh Dagh trough axis towards the Turanian foreland during the Mesozoic and Tertiary, based on changes in sedimentary thickness across the region. Therefore, the deflection of the East Alborz (Fig. 1c) probably began when the Kopeh Dagh basin began to be uplifted. The Kopeh Dagh range consists of uplifted Cretaceous limestone and overlying early-Alborz-derived molasse (e.g. continental red beds of the Palaeocene Pestehleigh Formation). The rocks are structurally distinct from those of Central Iran, lying north of the Palaeotethys suture, and are considered part of Eurasia based on the exposure of Eurasian Palaeozoic rocks in the Agdharband erosional window in the eastern Kopeh Dagh (Stöcklin 1968; Berberian & King 1981; Ruttner 1993; Alavi 1996). Gravity anomalies show that the adjacent flat Turkmenistan plain NE of the Kopeh Dagh is a filled-in flexural foreland basin (Maggi *et al.* 2000).

During the Middle to Late Miocene, further pulses in exhumation occurred in the west and central Alborz. Thermochronology studies record various ages for these pulses: 16 Ma and 7–8 Ma for samples spanning the west, central and central-east Alborz (Rezaeian 2008); 12 Ma for samples from the west Alborz (Guest *et al.* 2006b); and 6–4 Ma for samples from the central Alborz (Axen *et al.* 2001). It is thought the region underwent major tectonic reorganization between 15 and 5 Ma, during which full-scale Arabia–Eurasia continental collision and crustal thickening began (e.g. 10–14 Ma McQuarrie *et al.* 2003). The younger event at 5 Ma may correspond to the onset of seafloor spreading in the Red Sea (Hempton 1987). During the Late Miocene, shortening across the Kopeh Dagh in NE Iran is thought to have changed from predominantly folding and thrusting, to westward extrusion and the onset of subduction of the South Caspian-West Kopeh Dagh block (Hollingsworth *et al.* 2008). However, although the Kopeh Dagh form a seismically active and abrupt northeastern limit to active deformation in Iran, displaced Quaternary fans along the East Alborz, Sabzevar and Kuh-e-Sorkh mountain ranges indicates that present-day shortening is actually distributed across the entire NE Iran region. The aim of this paper is to investigate the active tectonics of NE Iran south of the Kopeh Dagh, and also to better quantify rates of shortening across each of the mountain ranges.

2.3 Seismicity

Unlike the Kopeh Dagh, the East Alborz have experienced no major destructive earthquakes over the last 150 yr, although three events for which fault plane solutions could be determined occurred on 1969 January 3 (M_w 5.5), 1987 April 10 (M_w 5.1) and 2003 July 3 (M_w 5.1)—see Fig. 2, and Table 1—for a summary of seismicity in the Kopeh Dagh, see Hollingsworth *et al.* (2006). Despite this relative seismic quiescence in recent times, destructive historical earthquakes near Neyshabur (1209, 1270, 1389 and 1405) and Esfarayen (1695) indicate that the East Alborz play an important role in accommodating regional shortening (Table 1 and Fig. 2). Near 61°E, the East Alborz range dies out along the Iran–Afghanistan border, before rising again as the E–W Paropamisus mountains of

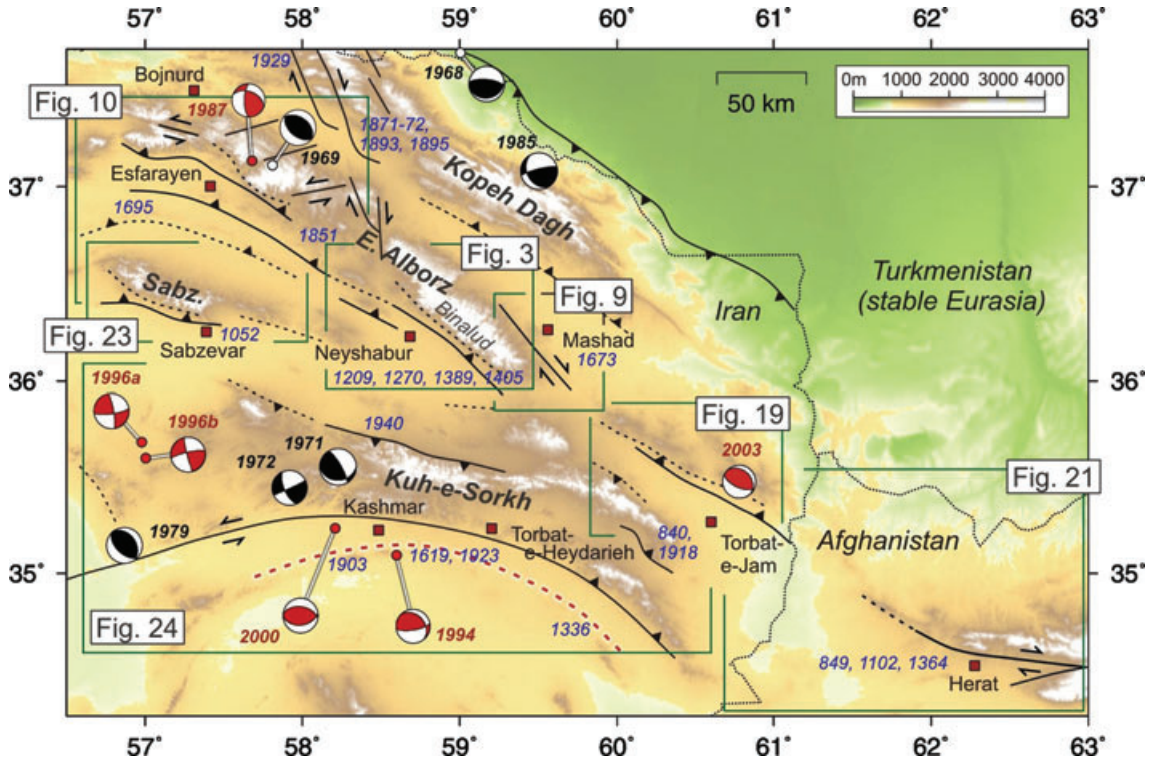

Figure 2. (a) Simplified seismotectonic map for the area of NE Iran east of 57°E and south of the Kopeh Dagh (see also Hollingsworth *et al.* 2006, 2008). Thrust faulting occurs along the south side of the East Alborz and Sabzevar ranges, and the north side of the Kuh-e-Sorkh range between 57 and 61°E (shown by black lines). Minor strike-slip also occurs along the the north side of the East Alborz range. Dotted black lines show older thrust faults (that may or may not be active) which lie within the East Alborz and Sabzevar mountains, as well as potentially active younger thrust faults in the intervening basin. Red dotted line highlights an active Neogene fold south of the Kuh-e-Sorkh range. Fault plane solutions for recent large earthquakes ($M_w > 5.1$) are shown in red (from the Harvard CMT catalogue), and black (Baker 1993). Dates are given for major historical earthquakes which have affected the Esfarayen, Neyshabur, Sabzevar, Kuh-e-Sorkh and Herat regions.

Northern Afghanistan (Fig. 1c). Despite the dramatic cut off in recent (post-1964) seismicity along the Iran–Afghanistan border, three historical earthquakes occurred in the western Paropamisus, near the city of Herat, in 849, 1102 and 1364 (Ambraseys & Bilham 2003) suggesting some active deformation is accommodated in NW Afghanistan. The seismicity of the Sabzevar range resembles that of the East Alborz; no large earthquakes have been recorded during the instrumental period, although a large earthquake destroyed the city and surrounding area in 1052 (Ambraseys & Melville 1982; Fattahi *et al.* 2006, see Fig. 2). The Kuh-e-Sorkh mountains have experienced many large, but generally less destructive earthquakes over both historical and recent times (Fig. 2 and Table 1). The majority of these events occur along the southern margin of the range, and are probably related to slip on the left-lateral Doruneh fault (e.g. Fattahi & Walker 2007) and shortening across a prominent E–W fold south of the range (dashed red line in Fig. 2). In this paper, we use satellite and field data, and Quaternary dating methods, to identify which faults in the East Alborz, Sabzevar and Kuh-e-Sorkh ranges either slipped in recent earthquakes, or contribute significantly to the late Cenozoic deformation across this region. We also investigate how East Alborz deformation continues eastward into Afghanistan, which is thought to be aseismic, yet displays clear faulting in the geomorphology and has a record of historical seismicity.

In the following sections, we identify active structures along the East Alborz range which may have caused large historical earthquakes near Neyshabur (Section 3) and both historical and recent earthquakes near Esfarayen (Section 3). In Section 4, we identify other active structures along the East Alborz range near Torbat-e-Jam, SE of Neyshabur (Fig. 2), which have not experienced large historical earthquakes, but appear active based on their geomorphology and minor seismicity. We also examine how the deformation extends eastward into the Paropamisus mountains of Afghanistan. Finally, in Sections 6 and 7, we briefly discuss the active tectonics of the Sabzevar and Kuh-e-Sorkh mountain ranges.

3 NEYSHABUR EARTHQUAKES (1209, 1270, 1389, 1405 AND 1673)

The city of Neyshabur (200 000 pop.) lies on the southern margin of the Binalud section of the East Alborz mountains (Figs 2 and 3a). It has been destroyed at least five times by major historical earthquakes in 1209, 1270, 1389 and 1405 and 1673 (Table 1, see also Berberian & Yeats 1999). Three large faults occur in the region (Fig. 3a), which extend 100 km along the south side of the Binalud mountains: the Binalud and North Neyshabur faults lie at the foot of the range north of Neyshabur (Section 3.1), and the Neyshabur fault lies within the valley west of Neyshabur (Section 3.2). Although the historical reports are not detailed enough to resolve which faults ruptured during each earthquake, the damage distribution broadly indicates that the 1209 and 1389 events may have ruptured the southern Binalud range front east of Neyshabur, and the 1270 and 1405 events west of Neyshabur. Initial results from Quaternary dating of displaced geomorphic markers are used to better constrain the Late Quaternary rate of shortening across the North Neyshabur fault (Section 3.1.2) and Neyshabur fault (Section 3.2.2).

Table 1. Significant earthquakes in NE Iran, south of the Kopeh Dagh, over the last 2000 yr.

Date	Time (local)	Latitude (°N)	Longitude (°E)	Approximate Location	Magnitude					Source
849	–	34.3	62.2	Herat	5.3	–	–	–	–	1,2
840.07	–	35.2	60.4	Torbat-e-Jam	6.5	–	–	–	–	1
1052.06.02	–	36.2	57.7	Sabzevar	7.0	–	–	–	–	1
1102.02.28	pm	34.4	62.2	Herat	5.3	–	–	–	–	1,2
1209	pm	36.4	58.7	Neyshabur	7.3	–	–	–	–	1,3
1270.10.07	pm	36.2	58.8	Neyshabur	7.1	–	–	–	–	1,3
1336.10.21	am	34.7	59.7	SE Torbat-e-Hey.	7.6	–	–	–	–	1
1364.02.10	–	34.9	61.7	Herat	5.8	–	–	–	–	1,2
1389.02	am	36.2	58.8	Neyshabur	7.3	–	–	–	–	1,3
1405.11.23	–	36.2	58.8	Neyshabur	7.4	–	–	–	–	1,3
1619.05	–	35.1	58.9	Kashmar	6.5	–	–	–	–	1
1673.07.30	–	36.3	59.3	Mashad	6.6	–	–	–	–	1
1695.05.11	am	36.8	57.0	Esfarayen	7.0	–	–	–	–	1
1851.06	pm	36.8	58.4	Esfarayen/Neyshabur	6.9	–	–	–	–	1,3
1903.09.25	01:20	35.18	58.23	Kashmar	6.1	–	–	–	–	1
1918.03.24	03:24	35.08	60.69	Torbat-e-Jam	5.9	–	–	–	–	1
1923.05.25	22:21:30	35.19	59.11	Torbat-e-Hey.	5.8	–	–	–	–	1
1940.05.04	21:01:59	35.76	58.53	N Kashmar	6.4	–	–	–	–	1
	Time (GMT)				M_w (Nm^{-1})	Depth (km)	Strike (°)	Dip (°)	Rake (°)	
1968.11.15	06:25:39	37.73	59.03	SE Kopeh Dagh	5.4	18	276	69	97	4,5
1969.01.03	03:16:40	37.06	57.82	Esfarayen	5.5	7	132	50	95	4,5
1971.05.26	02:41:46	35.53	58.20	Kashmar	5.6	13	89	26	32	4,5
1972.12.01	11:39:02	35.43	57.92	Kashmar	5.4	8	65	87	-25	4,5
1979.12.09	09:12:04	35.11	56.82	W Kuh-e-Sorkh	5.6	9	325	36	99	4,5
1985.08.16	10:46:50	37.09	59.31	SE Kopeh Dagh	5.5	9	256	80	56	4,5
1987.04.10	06:43:22	37.17	57.68	Esfarayen	5.1	5	292	45	30	4,6
1994.12.14	20:43:53	35.10	58.61	Kashmar	5.2	15	319	32	144	4,6
1996.02.25a	16:14:12	35.69	56.92	W Kuh-e-Sorkh	5.4	20	82	77	10	4,6
1996.02.25b	17:42:06	35.61	57.01	W Kuh-e-Sorkh	5.3	30	257	79	05	4,6
2003.07.03	14:59:30	35.41	60.76	Torbat-e-Jam	5.1	15	316	30	109	4,6

Notes: Historical earthquakes are from: (1) Ambraseys & Melville (1982); (2) Ambraseys & Bilham (2003); (3) Berberian & Yeats (1999). Instrumental earthquakes are from: (4) Engdahl *et al.* (2006); (5) Baker (1993) and (6) Harvard CMT (http://www.globalcmt.org/). The determination of Magnitude for historical earthquakes is based on written accounts of destruction, and consequently they represent poorly constrained estimates. Nevertheless, they are useful in identifying when significant earthquakes occurred prior to the instrumental period.

The damage distribution for the 1673 event, in which one third of Neyshabur and one half of Mashad was destroyed, led Berberian & Yeats (1999) to conclude that this earthquake probably ruptured a fault on the north side of the Binalud range in the vicinity of Mashad (Figs 2 and 3). A potential fault which may have ruptured during this earthquake is the Shandiz fault, which passes 10 km south of Mashad and strikes NW–SE (Fig. 3). This fault is discussed further in Section 3.3.

3.1 North Neyshabur fault

3.1.1 Geomorphology

North of Neyshabur city, the North Neyshabur and Binalud faults run parallel along the Binalud range front for 100 km (Fig. 3a). The North Neyshabur fault runs along the foot of the mountains, and has thrust Neogene deposits over the Neyshabur plain, forming a step in the topography of up to 300 m (Figs 3b–d). The Binalud fault lies 5 km to the north, and thrusts Jurassic metamorphic rocks over Neogene deposits. Both faults have relatively sinuous surface traces, typical of dipping thrust faults, and do not show any clear strike-slip component. A topographic profile across the range front is shown in Fig. 3(b). The region of uplifted Neogene rocks between the Binalud and the North Neyshabur fault forms a characteristic low step at the foot of the range, which has formed due to the basinward migration of thrust faulting. Similar examples are seen along the East Alborz at Esfarayen (Section 4.1) and Torbat-e-Jam (Section 5.1), as well as the Sabzevar mountains (Section 6, and elsewhere in Iran (e.g. Berberian *et al.* 2001; Walker *et al.* 2003). Basinward fault migration is typical of older continental thrust systems such as the Alps and Himalayas (Boyer & Elliott 1982; Hilley *et al.* 2005).

Fig. 4 shows a perspective view of the North Neyshabur and Binalud faults. As thrust faulting propagated southwards, Quaternary alluvial fans deposited south of the Binalud fault became uplifted, causing rivers to incise through them. Consequently, many Quaternary fan surfaces now occur across the region of uplifted Neogene rocks (e.g. Fig. 3d). Similar surfaces are not present north of the Binalud fault, which may be due either to relative inactivity on the Binalud fault or removal of the higher fan surfaces by erosion. However, because the fan surfaces south of the Binalud fault are so well preserved (i.e. have suffered little erosion), and the dramatic change in fan preservation coincides exactly with the Binalud fault trace, we suspect the North Neyshabur fault has accommodated the majority of regional shortening during the Quaternary. Nevertheless, the Binalud fault may still be active, as older bedrock mountain faults elsewhere in Iran are known to have ruptured in large thrust earthquakes (e.g. the 2005 Zarand earthquake, Talebian *et al.* 2006).

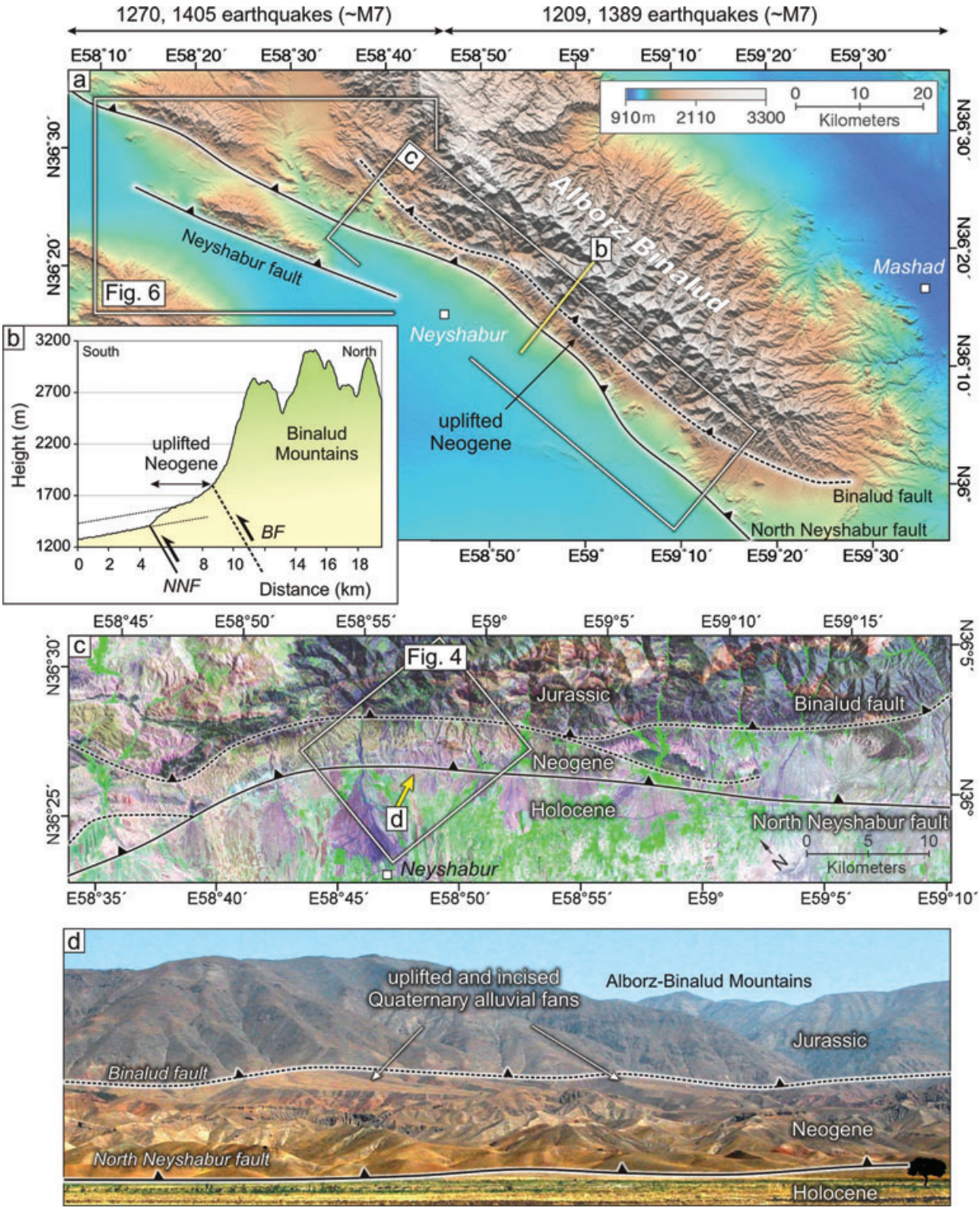

Figure 3. (a) SRTM digital topography of the Neyshabur region. Large historical earthquakes occurred to the west of Neyshabur in 1270 and 1405, and to the east in 1209 and 1389 (see text for details, and Berberian & Yeats 1999). Active faults are shown as black lines, less active faults are shown by dashed lines. The Binalud and North Neyshabur faults run parallel along the southern range front, north of the city, and the Neyshabur fault steps south of the range, west of the city. (b) Profile across the southern Binalud mountains (see yellow line in (a) for location), extracted from SRTM topographic data. Uplifted Neogene deposits form a low step at the foot of the high topography, bounded by the North Neyshabur (NNF) and Binalud (BF) faults. (c) False colour Landsat7 satellite image of the Binalud range front, north of Neyshabur city. The uplifted Neogene deposits form a distinctive 'yellow' band, between 'black' Jurassic shales of the high Binalud, and 'purple' Holocene gravels and 'green' cultivated regions of the low Neyshabur plain. Faults are shown as black lines. (d) Field photo looking north at the range front, from Neyshabur city (see yellow arrow in (c) for view direction). Within the mountains, the older Binalud fault is seen thrusting grey Jurassic shales over red Neogene conglomerates. Recent uplift on the North Neyshabur fault, which runs along the edge of the topography, has caused river incision, and the abandonment of alluvial fan surfaces.

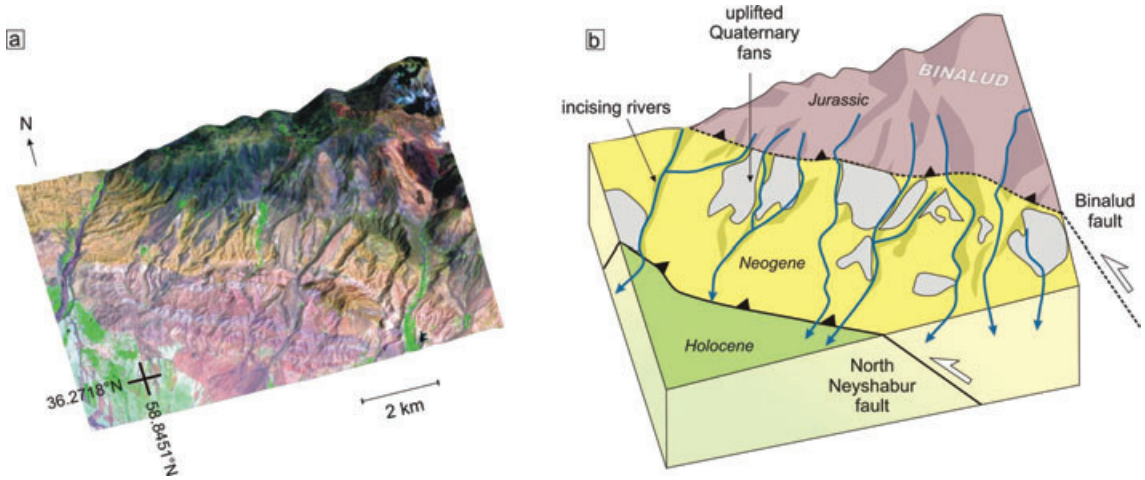

Figure 4. (a) Perspective view (Landsat7 draped over SRTM topography) of the southern Binalud range front, north of Neyshabur (see Fig. 3 for location). This is a typical view seen along the entire length of the range, and shows a low Neogene step formed by the migration of thrust faulting south of the high topography. (b) Schematic interpretation of the range front shown in (a). Jurassic shales (purple) are thrust over Neogene conglomerates (yellow) by the Binalud fault, and the Neogene over the Holocene plain deposits (green) by the North Neyshabur fault. Active river incision (blue lines) has formed a series of Quaternary terraces and uplifted alluvial fan surfaces (grey), which only occur south of the Binalud fault. This suggests the majority of Quaternary shortening is accommodated on the North Neyshabur fault.

3.1.2 Quantitative estimates of deformation

To determine the slip rate for a fault, the age, geometry and displacement of a geomorphic feature must be known. The last two may be determined from field observations, while the age must be determined using Quaternary dating techniques. At 36°18′N 58°50′E, the North Neyshabur thrust fault is exposed in a river section (Figs 5a–d). The fault dips 60° north and forms a 8 m high fault scarp at the surface (e.g. Figs 5d and f), which vertically offsets a Quaternary terrace (Fig. 5d). Colluvial deposits (7–8 m thick) in the footwall probably result from a number of earthquakes. Within the river section, a yellow sandstone unit is offset by 9 m. This value could not be measured directly, due to its high location within the river section, and so was determined from field photos containing a scale. A 60 × 40 cm sample of this unit was collected from the river exposure for optically stimulated luminescence (OSL) dating (the location of this sample, N5, is 36°18.309′N 58°50.270′E, see Figs 5c and d). A detailed account of the methodology is given in (Fattahi & Walker 2007). OSL dating measures the time since the sampled sedimentary material was last exposed to sunlight (assumed to be the time of deposition—see Appendix S2 for further details). The medium-fine grain size of sample N5 suggests the material was in transport for longer than the surrounding coarse gravels. Long transport times are desirable for luminescence dating, as the samples are more likely to have been exposed to sufficient sunlight required to excite all the trapped electrons to their original positions within the crystal lattice. If this is not the case, and the sample is not fully reset, the determined age will include an inherited component and will therefore overestimate the true age of deposition.

A wide palaeodose distribution for 18 subsamples of sample N5 (Fig. 5e) indicates the sediment may not have been completely reset upon deposition. This causes the mean age determination, 55.0 ± 21.3 kyr, to overestimate the real deposition age. One common solution to this problem is to assume the sample contains a proportion of fully reset grains amongst a mass of other grains which have been reset by varying degrees. Therefore, the youngest age determined from the palaeodose distribution curves will correspond to the grains in the sample which have been fully reset, and represent the time of deposition. However, even this minimum age determination method may overestimate the real deposition age as each subsample is also formed from a mixture of fully reset and partially rest grains. Nevertheless, this minimum age approach yields a lower age of 24.1 ± 1.9 ky from sample N5. Although we suspect the minimum age determination to more closely reflect the true age of deposition, we calculate the slip rate on the North Neyshabur fault using both minimum and mean age determinations (see Table 2). The fault slip rate determined using the minimum age of sample N5 is 0.3–0.4 mm yr^{-1}. This value represents a minimum estimate, because the fault has displaced younger overlying sediments by the same amount (9 m) as the N5 yellow sandstone unit. A more comprehensive dating study is required to better constrain the fault slip rate (which ideally includes multiple dating techniques, more samples, as well as a test of the stratigraphic succession, e.g. Nissen *et al.* 2009).

Although we do not know the age of the river terrace deposits which have been vertically displaced by 8 m at the surface (above the N5 sample location, Fig. 5c), we also calculate a possible slip rate for the North Neyshabur fault assuming this surface was abandoned at 11 ± 2 kybp (Table 2). This assumption is likely to be valid because: (1) the terrace must have been formed during a wet period younger than the 24.1 ky age of sample N5; (2) the last major wet period in NE Iran is thought to have coincided with the end of the last ice age at ∼11 kybp (Regard *et al.* 2005; Fattahi *et al.* 2006, 2007) and (3) this value marks the last regional incision event recognized in NE Iran, based on the 11 ± 2 ky age of the youngest displaced terrace deposits on the nearby Sabzevar thrust (Fattahi *et al.* 2006) and Doruneh fault (Fattahi *et al.* 2007), as determined by OSL dating. Assuming the top terrace is 11 ± 2 kyr, the North Neyshabur fault slip rate is still relatively low (i.e. <1 mm yr^{-1}).

To estimate the component of horizontal shortening across the North Neyshabur fault, knowledge of the fault geometry is required (see Appendix S3 for further discussion). In the river section shown

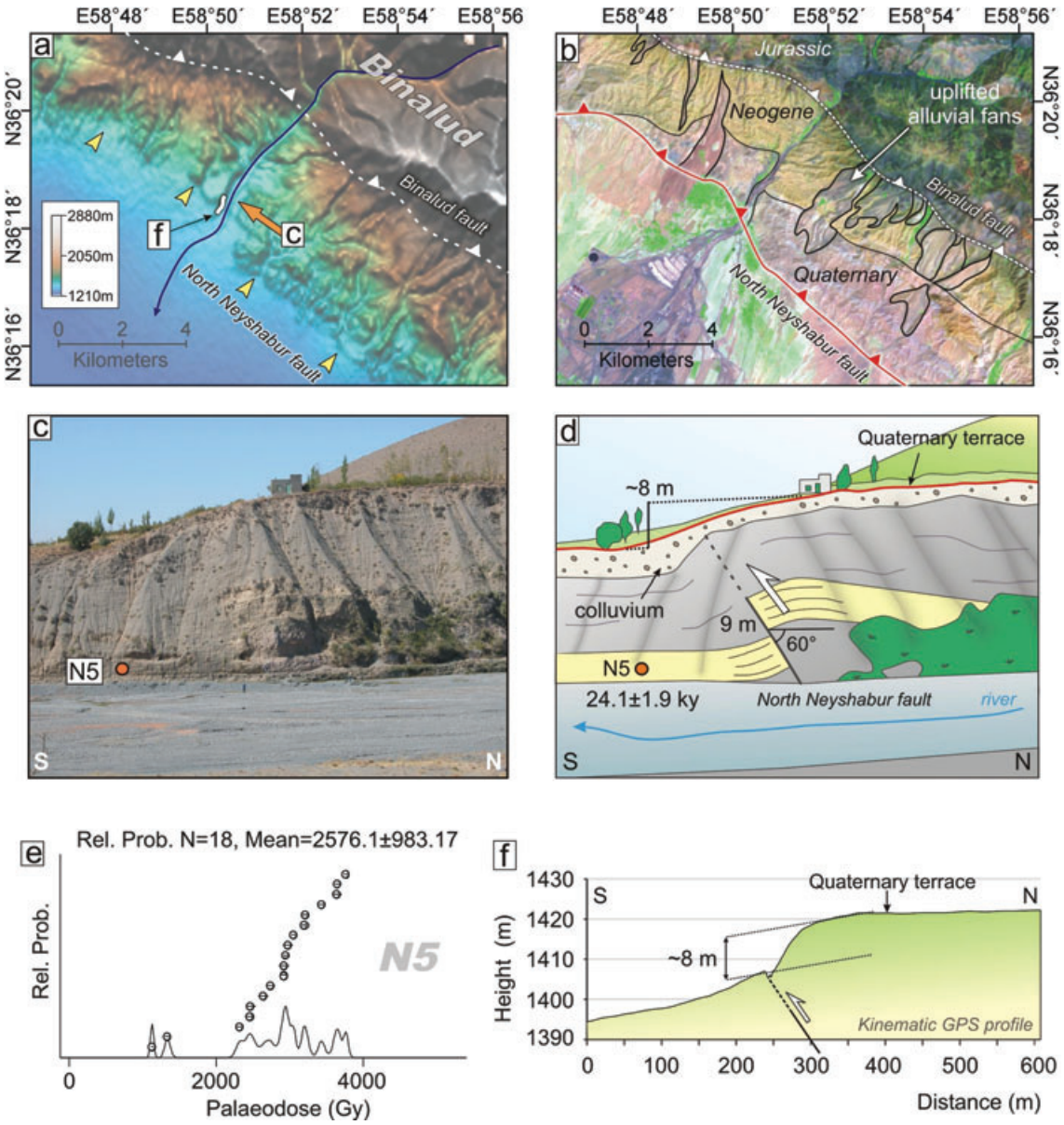

Figure 5. (a) Topographic map of the Binalud range front, north of Neyshabur (same location as Fig. 4). Blue line shows a large river, which drains south across the North Neyshabur fault and exposes it in section. Dashed white line shows the Binalud fault, and the yellow pointers mark the topographic step formed by the North Neyshabur fault. Orange arrow shows the location of the field photo shown in (c), and the white line shows the topographic profile shown in (f). (b) Landsat7 satellite image of the region in (a), for comparison. Lithologies are marked, and the North Neyshabur fault is shown in red. Uplifted Quaternary alluvial fan surfaces are outlined in black. (c) Field photo looking west from 36°15.967′ N 58°50.247′ E showing the North Neyshabur fault exposed in a river section. The orange circle shows the location of sample N5 (see text for details). (d) Schematic interpretation of field photo (c). The yellow sandstone deposits have been displaced 9 m by the North Neyshabur thrust. A similar displacement is seen in the Quaternary terrace at the surface. Thick colluvial deposits occur in the footwall, south of the fault. The minimum age determination of sample N5 is shown. (e) Palaeodose distribution curve for sample N5. The broad spread of data suggests the sample was not fully reset on deposition. (f) Topographic profile across the fault scarp shown in (d), obtained using kinematic GPS receivers—see (a) for location. The youngest terrace has been displaced vertically 8 m across the fault.

in Fig. 5(c), the fault dips north at 60°. If this dip is representative of the fault at depth, the shortening-rate is 0.3–0.5 mm yr^{-1}. However, if the fault shallows out at depth onto a horizontal décollement, then the shortening rate on the décollement will equal the fault slip rate where the fault ramps to the surface, that is, 0.7–1.0 mm yr^{-1} (see Appendix S3). To determine which shortening rate estimate is correct for the North Neyshabur fault knowledge is required of the subsurface structure across the fault, which may be revealed by seismic reflection experiments. As we lack this information, our estimate for the shortening rate across this fault incorporates both rates estimated above as upper and lower bounds, yielding 0.3–1.0 mm yr^{-1} (Table 2).

3.2 Neyshabur fault

3.2.1 Geomorphology

The Neyshabur fault strikes NW–SE for 50 km along the southern East Alborz range front, west of Neyshabur city (Figs 6a and b).

Table 2. Results from optically stimulated luminescence dating for sample N5. Fault slip, uplift and shortening rates for the North Neyshabur fault are calculated using both mean and minimum age determinations, and assuming a top terrace age of 11 ± 2 kyr for a 60° north-dipping fault.

Rate (mm yr^{-1})	Mean Age (55.0 ± 21.3 kyr)	Min. Age (24.1 ± 1.9 kyr)	Top Terrace (11 ± 2 kyr)
Fault Slip	0.1–0.3	0.3–0.4	0.7–1.0
Uplift[a]	0.1–0.2	0.3–0.4	0.6–0.9
Shortening[a]	0.1	0.2	0.3–0.5

[a]Assuming a 60°-dipping thrust fault.

The fault lies 10 km south of the North Neyshabur fault, and has thrust Eocene deposits and volcanics over the Neyshabur plain. The close proximity of this fault to Neyshabur city means it may have ruptured during the 1209–1405 earthquake sequence and poses a significant seismic risk to the city.

The Neyshabur fault is made up of three fault segments (Fig. 6a). The central segment is 30 km long and shows the greatest uplift, based on its topographic expression. Two smaller 10 km-long thrust segments occur either side of this central segment. Their low relief suggests they are young, and may possibly represent recent lateral propagation of the fault to the SE and NW. The SE segment of the Neyshabur fault passes through the village of Shori (Fig. 6a). Recent uplift of Quaternary river deposits north of the fault has formed a low ridge 40 m high. South-draining streams have incised where they cross the structure, and Quaternary gravels steepen along the southern margin of the fold (Fig. 6b). No exposures of the fault were found in the river sections crossing the fault, indicating slip on a blind thrust. The uplifted Quaternary deposits gradually decrease in height east and west of the structure, eventually merging with the active Neyshabur flood plain. This localized uplift is therefore likely to be of tectonic origin rather than a result in a change of the regional base level.

3.2.2 *Quantitative estimates of deformation*

Samples from the uplifted Quaternary deposits near Shori were collected for OSL dating (for locations, see Fig. 7a), to determine the slip rate for this segment of the Neyshabur fault. Sample N1 (Fig. 7b) was collected from Quaternary gravels in the highest central part of the fault segment. Samples N2 and N3 were collected from the eastern end of the segment, near the village of Sahlabad (Figs 7f and d, respectively). The vertical displacement across the fault was measured by kinematic GPS surveys for the N2 (12 m, see Fig. 7g) and N3 (7 m, see Fig. 7e) sample sites, and extracted from SRTM digital topography for the N1 sample site (35–45 m, see Fig. 7c). Although a lack of exposure prevented a convincing geological reconstruction across the fault, topographic offsets for each sample site likely represent the total vertical motion since the material was uplifted above the depositional Neyshabur plain. We also assume the regional base level has not significantly changed over the latest Quaternary, and erosion of the generated topography has also been minimal during this time. As with sample N5 from the North Neyshabur fault, the palaeodose distributions for N1–N3 were relatively broad, suggesting the samples were not fully reset, and the minimum age determinations should be used (Figs 7b, d and f). A fourth sample N4 was collected from a cutting west of the village of Shori (N36°17.938 E58°38.491, see Fig. 7 for location). However, the unusually young age determination of 1.4 ± 0.8 ky (average age method) or 100 yr (minimum age method) for this sample compared with samples N1–N3, suggests it has probably been affected by agricultural reworking (something we could not rule out in the field). We therefore omit the results of sample N4 from this discussion.

To estimate the fault slip and shortening rates from the uplift rate, the dip of the fault must be known. As this segment of the Neyshabur fault is blind and the dip of the homogenous Quaternary sediments in the fault hanging wall could not be established, an estimate of the fault geometry is obtained using an elastic dislocation model to reproduce the topography created by slip on the fault, following the

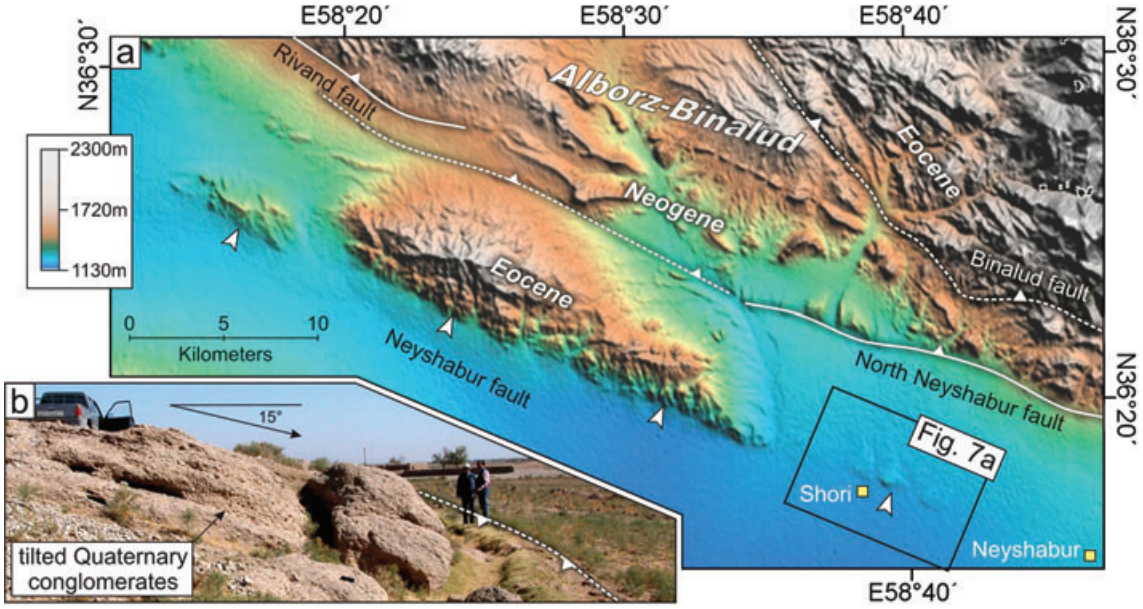

Figure 6. (a) Topographic map of the region west of Neyshabur, with faults shown as white lines. White pointers mark a step in topography formed by the Neyshabur fault. The village of Shori lies at the eastern end of the Neyshabur fault. (b) Field photo showing a view east (from N36°17.725′ N and 58°38.460′ E) along the eastern Neyshabur fault segment near Shori village. Recent uplift has resulted in the southward tilting of Quaternary conglomerates along the fault trace.

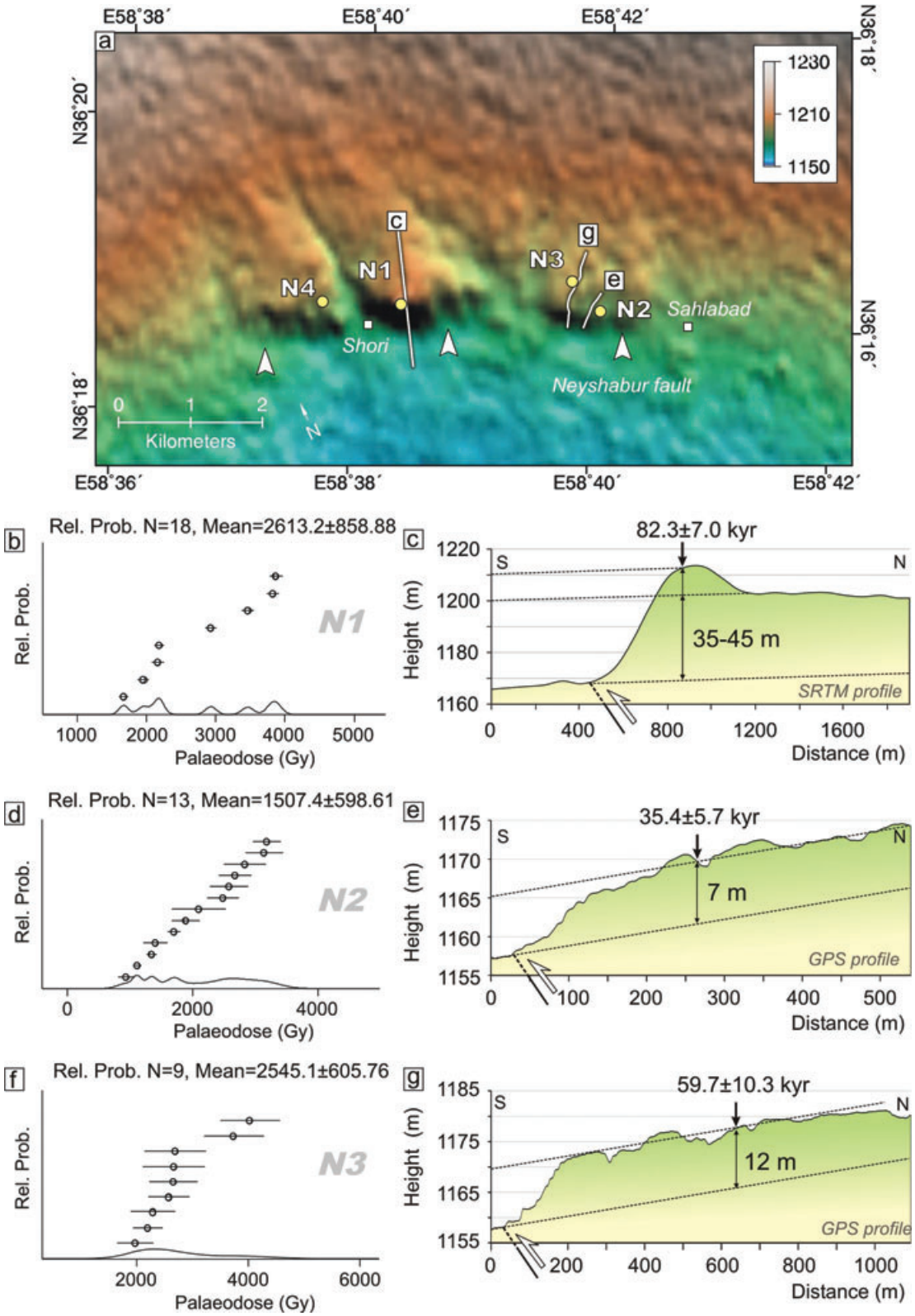

Figure 7. (a) Topographic image of the eastern Neyshabur fault segment near Shori, marked by white pointers. Yellow circles show the location of samples sites: N1, N2, and N3, from which uplifted Quaternary river deposits were collected for OSL dating (location of sample N4, which did not yield a sensible age, is also shown). White lines show topographic profiles taken across the fault. (b, d and f) Palaeodose distributions for samples N1, N2 and N3—see text for discussion. The units on the x-axis represent the number of seconds of exposure to a known beta source (in this case providing 5 Gy/min) required to reproduce the natural luminescence signal. The diagrams provide a visual measure of the degree of resetting of the luminescence signal on deposition. (c, e and g) Topographic profiles across the Neyshabur fault, taken at each sample site. The vertical offset is shown in each case. Profile (c) was extracted from SRTM digital topography, and profiles (e) and (g) were measured using kinematic GPS.

Table 3. Results from optically stimulated luminescence dating for samples N1, N2 and N3. Fault slip, uplift and shortening rates for the Neyshabur fault are calculated using both mean and minimum age determinations, and a fault dip of 60°.

	Rate (mm yr^{-1})	Mean age (129.0 ± 43.5 ky)	Minimum age (82.3 ± 7.0 ky)
	Fault Slip[a]	0.2–0.6	0.5–0.7
N1	Uplift	0.2–0.5	0.4–0.6
	Shortening[a]	0.1–0.3	0.2–0.3
		(56.9 ± 22.9 ky)	(35.4 ± 5.7 ky)
	Fault Slip[a]	0.1–0.2	0.2–0.3
N2	Uplift	0.1–0.2	0.2
	Shortening[a]	0.1	0.1
		(76.6 ± 18.8 ky)	(59.7 ± 10.3 ky)
	Fault Slip[a]	0.1–0.2	0.2–0.3
N3	Uplift	0.1–0.2	0.2
	Shortening[a]	0.1	0.1

[a]Assuming a 60°-dipping thrust fault.

approach of King *et al.* (1988) and Stein *et al.* (1988); see Appendix S4. It is found that the morphology of the Neyshabur fault segment near Shori is fitted best by a steeply dipping fault (60–80°), and the small wavelength of the fold suggests a shallow depth of faulting (1–2 km). This raises the possibility that the Neyshabur fault splays out from the North Neyshabur fault on a shallow décollement. The rate at which the fault slips on the horizontal décollement may be calculated in the same way as for the North Neyshabur fault (Section 3.1.2), the results of which are shown in Table 3. Since we cannot rule out the Neyshabur fault cutting the entire crust we also calculate the rate of horizontal shortening (x) by resolving the uplift rate (y) onto the fault plane to give the fault slip rate (z), and then taking the horizontal component of motion. Furthermore, we can not rule out slip on a décollement which does not ramp to the surface, i.e. uplift resulting from fault tip folding (e.g. Daëron *et al.* 2007), since the fault is not exposed along the southern limit of the Shori fold.

If the décollement occurs at 1.5 km depth (as indicated by our dislocation model), we can estimate the amount of shortening required to produce the observed uplift using a simple mass balance approach (Daëron *et al.* 2007) shown in Fig. 8; this method yields a shortening rate of 0.27 mm yr^{-1} and is consistent with the estimates shown in Table 3.

Slip rates determined using both the mean and minimum age determinations do not differ dramatically and in all cases are $<$1 mm yr^{-1}. However, sample N1 gives slightly older ages than N2 and N3. This may be due to the location of sample N1 which comes from the middle of the fault segment, which gets uplifted above the active flood plain first, whereas samples N2 and N3 come from the eastern tip of the fault segment, which was uplifted above the active flood plain more recently (based on a lateral fault growth model). Therefore, the values obtained using sample N1 are considered more representative for this segment of the Neyshabur fault, that is, a horizontal shortening rate of 0.5–0.7 mm yr^{-1} assuming extrusion of material on a décollement and ramp structure. However, a more conservative estimate of 0.1–0.7 mm yr^{-1}, which takes into account all the possible shortening estimates in Table 3 may be more suitable. These values are similar to the North Neyshabur fault slip rate calculated in Section 3.1.2 Therefore, the combined rate of shortening across both of these thrust faults is 0.4–1.7 mm yr^{-1}, and is likely to represent the Holocene shortening rate across the entire East Alborz range at the longitude of Neyshabur.

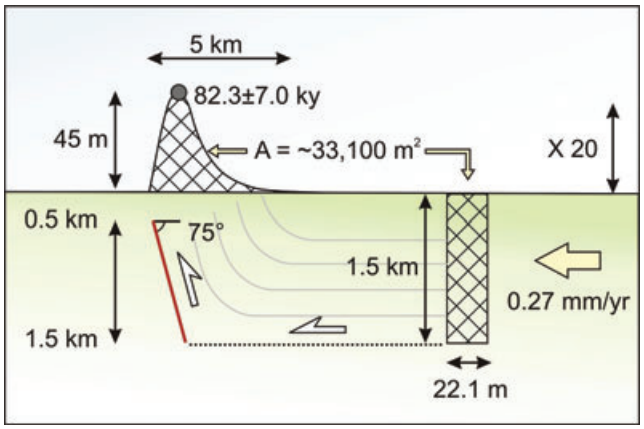

Figure 8. Schematic geological cross section across a décollement which ramps towards the surface on a steeply dipping (75°) blind thrust between 0.5 km and 1.5 km depth. Over time, slip on the fault results in an asymmetric fold at the Earth's surface. The cross sectional area of this fold may be calculated from a topographic profile, and is approximately 33,100 m^2. If this amount of material has been extruded only by slip above the décollement, which extends to a depth of 1.5 km, the equivalent amount of shortening on the décollement required to produce the fold is 22.1 m. If this value represents the total amount of horizontal shortening since Quaternary deposits in the crest of the fold were deposited prior to uplift (82.3 ± 7.0 ky), the rate of shortening across the structure is 0.27 mm yr^{-1}. Although this estimate is poorly constrained, it likely represents a minimum value of shortening as it ignores any erosion which may have resulted in the redistribution of material away from the fold.

3.3 Shandiz fault and the 1695 Mashad earthquake

The Shandiz fault strikes NW–SE for 100 km along the north side of the East Alborz, 10 km southeast of Mashad (Fig. 9a). A large M6–7 earthquake in 1673 July 30 destroyed two thirds of Mashad (including the dome over the tomb of Imam Reza), killing ∼4000 people (Ambraseys & Melville 1982). The location of this earthquake (Fig. 9a), based on historical records of structural damage, is poorly constrained. However, it may have occurred on the Shandiz fault, which is the only known large active fault close to Mashad.

Minor vertical displacement occurs across the fault, and the linear strike of the fault trace across the topography suggests a steeply dipping fault plane. Right-lateral displacement of a terrace riser by 5 m, shown in Fig. 9(b), may represent a coseismic rupture dating from the 1673 earthquake. The geomorphology of this fault indicates some right-lateral shear is accommodated on the southern side of the SE Kopeh Dagh.

4 ESFARAYEN EARTHQUAKES 1695, 1969, AND 1987

The city of Esfarayen (130 000 pop.) lies on the south side of the East Alborz near 57°30′E (Fig. 10). A large (M 7.0) earthquake affected the region in 1695 May 11, which destroyed several villages in the valley south of Esfarayen, with casualties ranging from 10 to 100 in each one (Ambraseys & Melville 1982). Land sliding was reported in the surrounding mountains, and strong aftershocks continued for a year. The large number of seismogenic structures in the Esfarayen region make it difficult to identify which fault ruptured during this earthquake (Fig. 10).

Two recent earthquakes occurred in the East Alborz mountains north of Esfarayen on 1969 January 3 (M_w 5.5) and 1987 April 10 (M_w 5.1). Although these events are relatively small, the resulting

Figure 9. (a) Landsat7 satellite image of the region south of Mashad (see Fig. 2 for location). The NW–SE Shandiz fault cuts along the edge of the Binalud mountains (marked by white pointers). Although the fault displaces geology in a lateral way, the sense of motion cannot easily be determined due to the parallel strike of the geology with the fault. The approximate location of a large earthquake which destroyed Mashad in 1673.07.30 is shown by a yellow star. This event probably occurred on the Shandiz fault, as it the only large fault in the Mashad area. (b) Ikonos satellite image (©2010 Google, ©2010 GeoEye) of the region shown by the yellow circle in (a). The Shandiz fault runs across young Quaternary river deposits between the two black arrows. The black circle highlights an area of this fault, which has offset a stream in a right-lateral sense by 5 m. Inset shows simplified sketch of the offset river in (b). Yellow areas are low, containing streams which drain north. The regional slope direction is south-to-north. The fault has caused a small reversal in the topography, which is visible as a small ridge on the north side of the fault. The terrace risers have been offset by 5 m.

fault plane solutions provide information on the style of deformation across the range. The solution for the larger 1969 event has been constrained by body waveform modelling, and indicates NE-directed shortening across the range (see Section 4.1 for further discussion). The waveforms for the 1987 event were too small to be modelled in this way, and therefore the Harvard solution is shown in Fig. 10. Nevertheless, the slip vectors indicate predominantly strike-slip motion, either right-lateral (across-strike) motion, similar to the 1969 event, or left-lateral (along-strike) motion.

In the Esfarayen region a large number of faults show signs of activity in the Quaternary geomorphology (Fig. 10). Near Esfarayen city, the southern margin of the East Alborz mountains is formed by two large NW–SE thrust faults (the Esfarayen and North Esfarayen faults—Fig. 11(a), and Section 4.1). To the west, thrust faulting continues along an E–W striking fault (West Esfarayen fault—Fig. 13, and Section 4.2). Active left-lateral faults are present on the northern side of the East Alborz mountains, which are possibly conjugate to the right-lateral faults of the Central Kopeh Dagh to the north. South of the East Alborz, two 100-km-long thrust faults splay out from the range towards the west, forming low parallel ridges across the plain (the Rivand fault—see Section 4.4; and the Samghan fault—see Section 4.5).

4.1 Thrust faulting near Esfarayen

The faulting near Esfarayen city closely resembles that of Neyshabur, showing a migration of thrust faults into the basin. The Esfarayen fault lies at the foot of the range and has uplifted a sequence of Neogene terrestrial deposits, which form a low 300 m step in the topography (Figs 11a and b). Quaternary activity on this fault is indicated by a series of uplifted alluvial fan surfaces which overlie the Neogene deposits (Figs 11c and d). In the east, an older parallel thrust lies a few kilometres to the north (the North Esfarayen fault), which has thrust Jurassic limestones over the Neogene deposits. Displaced river terraces and alluvial fan surfaces are not present north of this fault, indicating that the majority of Quaternary shortening has occurred on the Esfarayen fault. A small Quaternary ridge south of the Esfarayen fault may represent another phase of thrust migration to the south (Fig. 11a). In the west, north of Esfarayen, the majority of Quaternary shortening has occurred on the Esfarayen fault and the Sast fault, which lies immediately south of the North Esfarayen fault.

The 1969 January 3 earthquake occurred approximately 15 km north of the range front (Fig. 11a), and may have involved rupture of the north-dipping Esfarayen fault, to which it projects at the surface (based on the strike: 304°, dip: 40°, rake: 95° and depth: 7 km determined by body waveform analysis, see Baker 1993, although error in the location may be up to 15–20 km). The slip vector of this earthquake indicates shortening perpendicular to the range, consistent with the Quaternary geomorphology of the Esfarayen fault, which shows a significant vertical and negligible lateral displacement.

The western end of the Esfarayen fault steps out from the high topography by 10 km (compared with 2 km further east). Recent activity on this fault is again indicated by the uplift of Neogene deposits

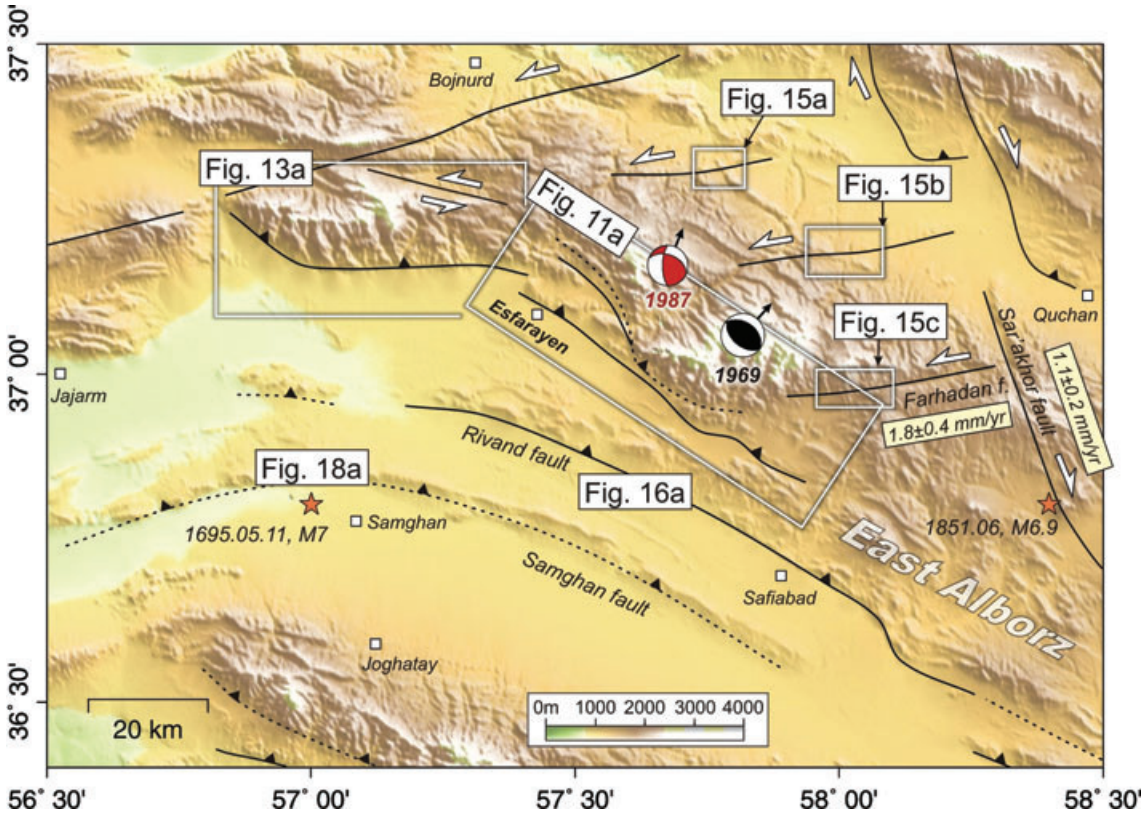

Figure 10. Topographic map of the Esfarayen region. Active faults (shown in black) are discussed separately in the text. Large historical earthquakes occurred in 1695 (M 7) and 1851 (M 6.9). Although the locations are very poorly constrained, they may have ruptured the Samghan and Rivand faults, respectively (see also Berberian & Yeats 1999). Ambraseys & Melville (1982) locate the 1695 earthquake near 36.8°N 57.0°E, near the Samghan fault. The Harvard CMT fault plane solution is shown in red for the 1987 earthquake, and the body waveform modelled solution of Baker (1993) is shown in black for the 1969 event (see also Table 1). In both cases the likely slip vector (south relative to north) is shown by a small black arrow.

by 100 m, which are overlain by Quaternary gravels (Fig. 12b). Furthermore, fault propagation to the west has resulted in the deflection of two large rivers, which drain south from the high East Alborz, leaving a series of dry valleys within the Neogene and Quaternary deposits (Figs 12a and d). Between the Esfarayen and North Esfarayen faults, the Sast fault has further uplifted Neogene and Quaternary deposits, causing river incision and terrace formation (Figs 12c and e). As these faults have migrated southwards, they have become more oblique to the range. This may result from the evolution and gradual clockwise rotation of the older faults away from their optimum orientation.

Recent movement on the Esfarayen fault has resulted in the uplift and formation of Quaternary terraces and displaced alluvial fan surfaces, similar in appearance and relative spacing to those seen at Neyshabur. This suggests that shortening across the East Alborz mountains near Esfarayen may be of the same order as at Neyshabur, that is, 1–2 mm yr^{-1}, although this estimate is poorly constrained.

4.2 Thrust faulting west of Esfarayen

West of Esfarayen, the East Alborz range front strikes E–W, and is bounded by the West Esfarayen thrust fault (Fig. 13). West of 57°E, this fault strikes NW–SE, which is more typical of the range east of Esfarayen. The fault forms a sharp topographic step along which Jurassic limestones and shales are thrust over the Esfarayen plain (Fig. 13a). Uplift north of the fault has caused rivers to incise through Quaternary alluvial fans, draining south from the high mountains (Fig. 13b). A small left-lateral component is also indicated by *en echelon* fractures formed where the fault cuts young alluvial deposits (Fig. 13c).

North of the West Esfarayen fault lies the Gerivan fault, which cuts across the high East Alborz mountains. The fault strikes linearly across the topography (Fig. 13a), and has produced a small reversal in slope near Gerivan village (Fig. 14a). Cultivation in the valley has obscured much of the recent fault geomorphology. Nevertheless, the restoration of a river 10 km east of Gerivan indicates a possible ∼700 m of recent left-lateral motion. Furthermore, the fault strike and sense of slip (left-lateral with a thrust component, N-side up) are similar to the fault plane solution for the 1987 earthquake, which occurred 25 km along strike to the SE (Fig. 10). However, it is not clear if this earthquake has been mislocated, or if it ruptured a different structure to the SE. The significance of the left-lateral Gerivan fault, which lies directly north of the E–W West Esfarayen thrust, may be that the overall direction of shortening is towards the NNE or NE, rather than N–S in this region. Nevertheless, the geomorphology, seismicity and GPS data are not sufficiently clear to rule out right-lateral slip on this fault, which would imply a regional NNW shortening direction across this part of the range.

4.3 Left-lateral faulting north of Esfarayen

The northern side of the East Alborz mountains, at the longitude of Esfarayen, is cut by a series of ENE–WSW left-lateral strike-slip

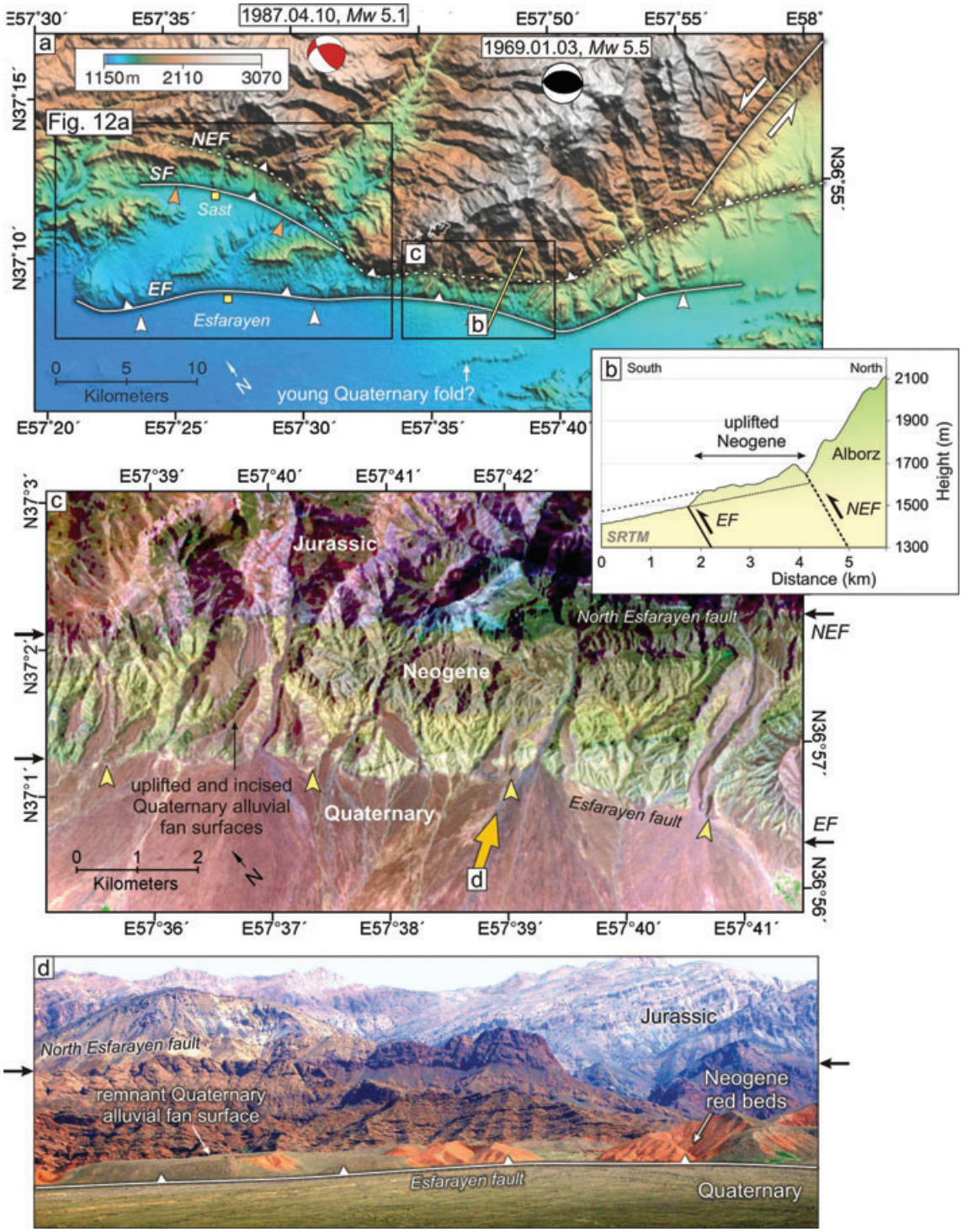

Figure 11. (a) Topographic map of the southern Alborz range front near Esfarayen. Three faults occur in the region (shown by white lines): the Esfarayen; Sast; and North Esfarayen faults. Fault plane solutions for two recent earthquakes are shown (red comes from the Harvard catalogue, and black is a body-wave modelled solution from Baker 1993). (b) Topographic profile along the range front (see (a) for location), which shows a low Neogene step at the base of the topography. Esfarayen (EF), Sast (SF), and North Esfarayen (NEF) faults are labelled. (c) Landsat7 satellite image of the range front southeast of Esfarayen. Faults are shown between the small black arrows at the sides of the image; the Esfarayen fault is also highlighted by yellow pointers. Quaternary shortening has occurred on the Esfarayen fault, causing river incision, and the uplift and abandonment of alluvial fans. The orange arrow shows the location of field photo (d). This view is taken from 36°56.78′ N 57°38.77′ E, looking north at the Alborz range front. The solid white line shows the Esfarayen fault running along the base of the mountains. Uplifted and incised alluvial fans are clearly visible as flat surfaces overlying dipping Neogene red beds. The older North Esfarayen fault strikes across the range behind the red Neogene ridge between the black arrows.

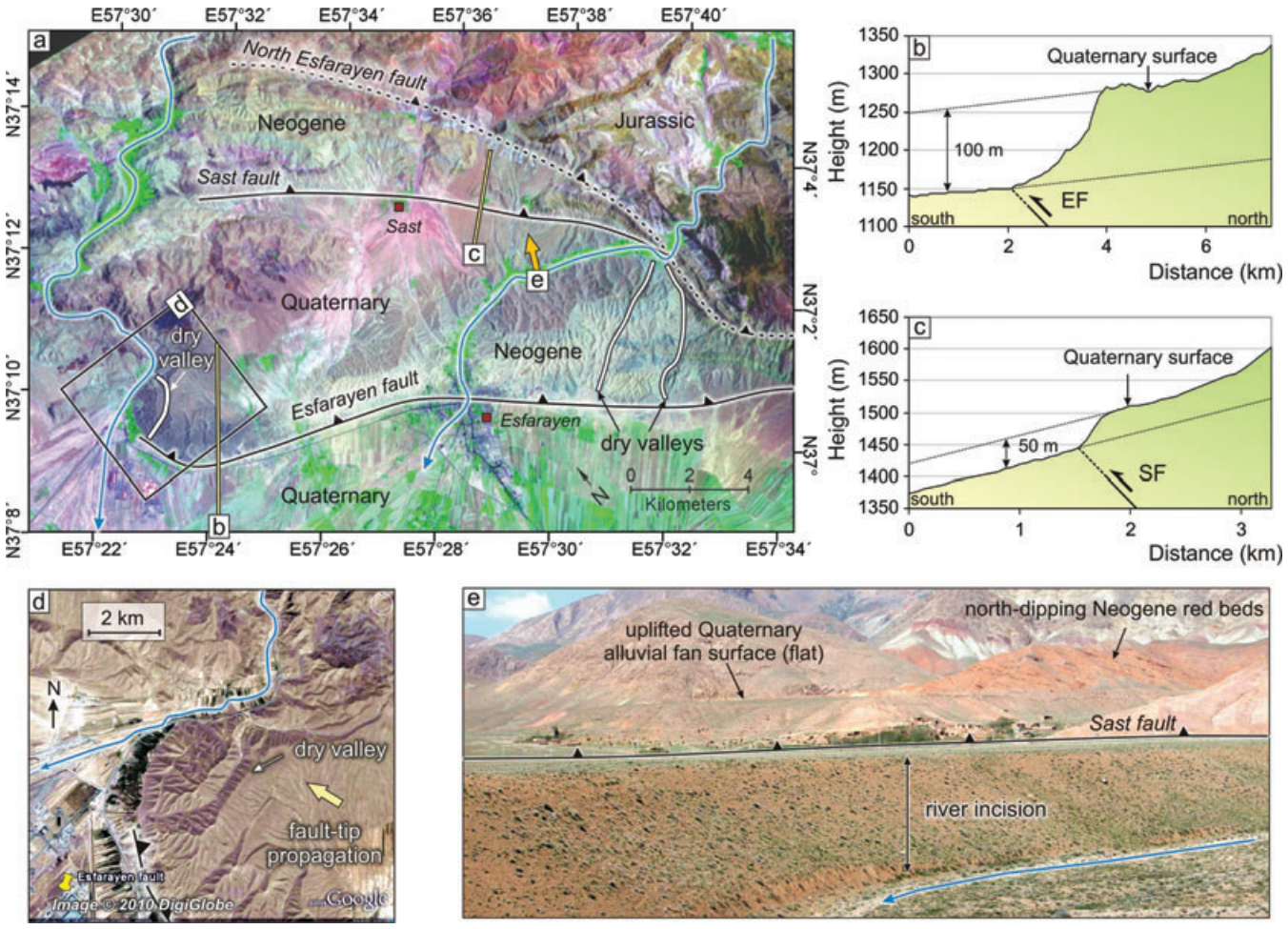

Figure 12. (a) Landsat7 satellite image of the western end of the Esfarayen fault (active faults are shown in black). Blue lines show major rivers draining south of the Alborz, which have been deflected by the northwest propagation of the Esfarayen fault, leaving a series of dry valleys (heavy white lines). The orange arrow shows the location of field photo (e). The location of topographic profiles, (b) and (c) are shown in yellow. These profiles are taken across Quaternary fan surfaces displaced across the Esfarayen fault (EF—100 m) and the Sast fault (SF—50 m), respectively. (d) Quickbird satellite image (©2010 Google, ©2010 DigitalGlobe) of the western end of the Esfarayen fault (see (a) for location), where uplift has caused the deflection of a river (blue line) to the west, and the abandonment of its original course which is now a dry valley. (e) Field photo looking north from 37°07.25′N 57°33.75′E at the Sast fault (black line), which has uplifted Quaternary alluvial fan surfaces to the north. Incision south of the fault is the result of uplift caused by the Esfarayen fault, which lies 5 km to the south.

faults, which strike linearly across the topography from the Atrak valley (Fig. 10). At least three faults occur, each extending for at least 20 km from the valley into the high topography. Examples of displaced geology and geomorphology from each fault are shown in Fig. 15. The two northern faults (Figs 15a and c) displace Cretaceous limestone on both sides of the fault, and therefore the total offset is hard to determine. Nevertheless, the truncation of a small anticline in Fig. 15(a), and deflected and abandoned drainage in Fig. 15(c), indicate offset of a few kilometres. The southern fault, known as the Farhadan fault (Shabanian *et al.* 2009a) displaces Eocene volcanics by 4 km, and Quaternary movement has deflected drainage against the general topographic slope by 1.5 km. Shabanian *et al.* (2009a) estimate a slip rate of 1.8 ± 0.4 mm yr^{-1} for this fault based on the offset of drainage and Pliocene deposits along the fault. Similar left-lateral faults are present further west along the Atrak valley near Bojnurd (Hollingsworth *et al.* 2008).

4.4 South Esfarayen: the Rivand fault

The Rivand fault runs along the southern East Alborz range front for 100 km between Esfarayen and Neyshabur (Fig. 16a). The fault has uplifted Eocene volcanics and Neogene deposits forming a 200 m-high ridge, which splays out from the range south of the Esfarayen fault. Recent activity on this thrust fault is indicated by uplifted Quaternary surfaces to the north, which lie up to 200 m above the valley floor (Fig. 16b). Furthermore, river profiles extracted from SRTM topography (e.g. Fig. 16c) show a 20 m step in gradient across the fault.

Directly south of Esfarayen, a sequence of Neogene sandstone, marl, conglomerate and volcanic rocks have been uplifted into a fold, which is truncated on its south side by the western end of the Rivand fault (Fig. 17a). Recent uplift has resulted in river incision and the formation of Quaternary terraces across the fold (Fig. 17b).

The geomorphology of the eastern end of the Rivand fault, near Safiabad also indicates activity in the Quaternary period (Fig. 17c). Recent uplift has caused rivers to incise through Eocene marls and conglomerates (Tatavousian *et al.* 1993), leaving a series of Quaternary river terraces and abandoned alluvial fan surfaces north of the fault (Figs 17c and d).

The low topography generated by the Rivand fault suggests it is a relatively young tectonic feature. Furthermore, the fault is located south of the Esfarayen fault, and splays out from the Alborz

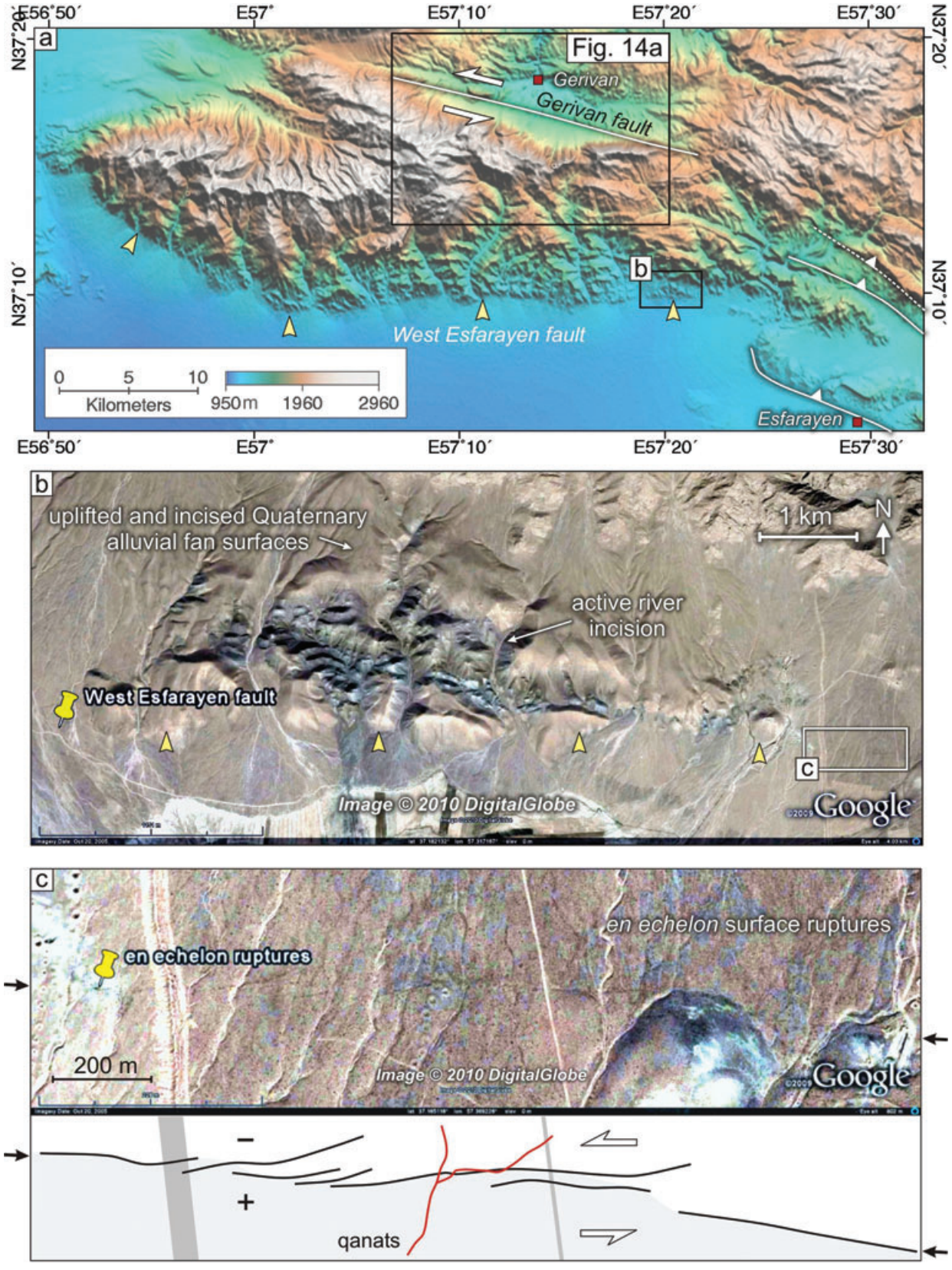

Figure 13. (a) Topographic map of the Alborz range front west of Esfarayen. A sharp step in the topography, marked by yellow pointers, corresponds to the West Esfarayen thrust fault. The left-lateral Gerivan fault strikes across the mountainous topography to the north. (b) Quickbird satellite image (©2010 Google, ©2010 DigitalGlobe) of the West Esfarayen fault. A significant shortening component exists on this fault, which has resulted in the uplift and incision of a series of alluvial fans. (c) Where the fault crosses the youngest fan deposits (i.e. between the two black arrows), *en echelon* cracks, indicating left-lateral motion, have formed. Qanat systems run along and across the fractures, tapping the ponded water (see also Jackson 2006).

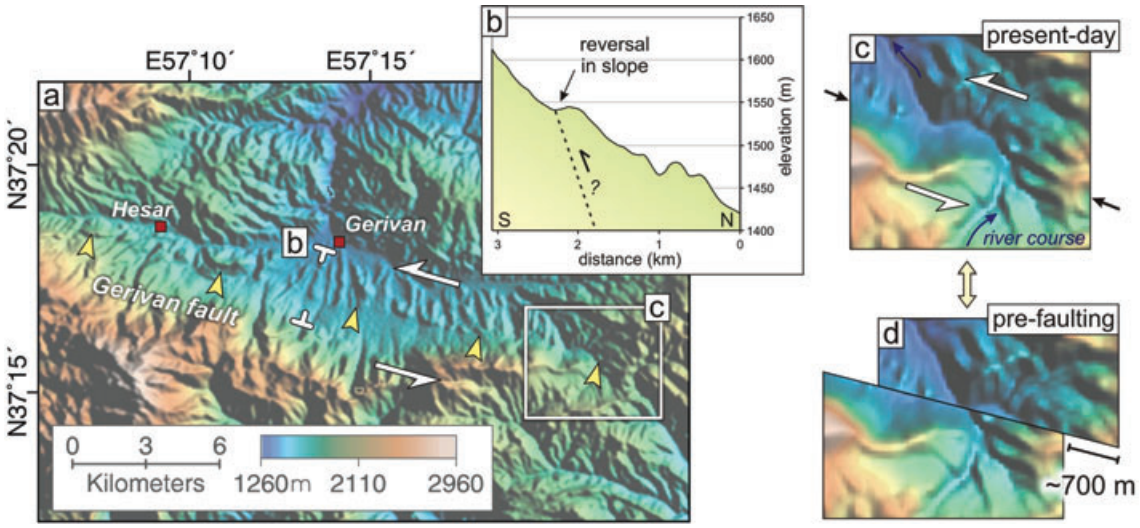

Figure 14. (a) Topographic map of the Alborz near Gerivan and Hesar villages (red squares). The Gerivan fault is highlighted by yellow pointers, and runs along the edge of the high topography in the southern half of the image. The fault has a small vertical component (up to the north), which has resulted in a small reversal in slope 2 km south of Gerivan village, as shown in the topographic profile (b). The linear strike of the Gerivan fault across the high topography may also suggest a steeply dipping fault plane typical of strike slip faults. (c and d) Possible left-lateral displacement of a river by ∼700 m along the SE end of the fault (see (a) for location).

mountains. These features suggest the Rivand fault may have formed during a recent phase of basinward thrust migration away from the main Alborz range.

4.5 South Esfarayen: the Samghan fault

Shortening in the Late Cenozoic has produced a 100 km-long E–W arcuate Neogene fold 20 km south of the Rivand fault (Figs 10 and 18). The fold rises 200 m above the surrounding plain, and has been produced by slip on the north-dipping and predominantly blind Samghan thrust fault, which projects to the surface along the southern edge of the fold. Near the village of Samghan, the fault has produced a small scarp which crosses a series of Quaternary alluvial fans uplifting them to the north (Fig. 18b). The Samghan fault is probably a young tectonic feature, as it only affects Late Cenozoic geology, and has generated little topography. Furthermore, it is less clearly expressed in the Quaternary geomorphology than the Esfarayen and North Neyshabur faults to the north. It therefore probably accommodates only a small amount of the regional shortening.

5 ACTIVE SHORTENING IN THE EAST ALBORZ BETWEEN NEYSHABUR AND HERAT, AFGHANISTAN

In this section, we combine recent seismicity with remote observations of the geomorphology to describe the active deformation of the East Alborz mountains near the city of Torbat-e-Jam (Section 5.1), which lies SE east of Neyshabur (Fig. 2). We also investigate whether active deformation continues along-strike to the east, where three large historical earthquakes damaged the city of Herat in NW Afghanistan (Section 5.2).

5.1 Torbat-e-Jam

The city of Torbat-e-Jam (60 000 pop.) lies south of the East Alborz mountains near the Iran–Afghanistan border (Figs 2 and 19a). Although no destructive earthquakes have affected this part of the range in historical or recent times, a relatively small thrust event on 2003 July 3 (M_w 5.1) indicates the range is actively accommodating regional shortening. The range front resembles that of Neyshabur and Esfarayen; a band of Neogene deposits, which have been uplifted by the Torbat-e-Jam thrust, forms a low step at the foot of the high topography (Figs 19a and b). A fault (here named the North Torbat-e-Jam fault) occurs to the north, which has thrust Jurassic shales and sandstones over the Neogene deposits to the south (Fig. 19b). Quaternary activity has occurred on the younger Torbat-e-Jam thrust, which has migrated into the foreland, causing rivers to incise through the Neogene deposits, and leaving a series of abandoned alluvial fan surfaces which overly the uplifted Neogene deposits (Fig. 20).

5.2 Herat

An important question regarding the active tectonics of NE Iran is whether the accommodation of Arabia–Eurasia shortening at the present day extends eastwards into Afghanistan. The city of Herat (350 000 pop.) lies 170 km southeast of Torbat-e-Jam, along the southern side of the Paropamisus mountains, which strike E–W across northern Afghanistan (Figs 2 and 21a). The Paropamisus have much in common with the East Alborz; they share a similar pre-Jurassic structural history (e.g. Şengör 1987; Golonka 2004; Natal'in & Şengör 2005), having formed during the Cimmerian Orogeny when the Helmand block was sutured to Eurasia along the PTS (see also Section 2.2). The East Alborz also appear topographically continuous with the Paropamisus, although the topography decreases significantly in the region between the two ranges, near the border between Iran and Afghanistan (Fig. 21b). Recent work by the USGS has gone some way to improving our understanding of the tectonics and geology of Afghanistan (Doebrich & Wahl 2006; Ruleman *et al.* 2007). Nevertheless, the Late Cenozoic tectonics of NW Afghanistan remain enigmatic, in particular how the small number of earthquakes relate to active structures, and how these structures accommodate either India–Eurasia or Arabia–Eurasia

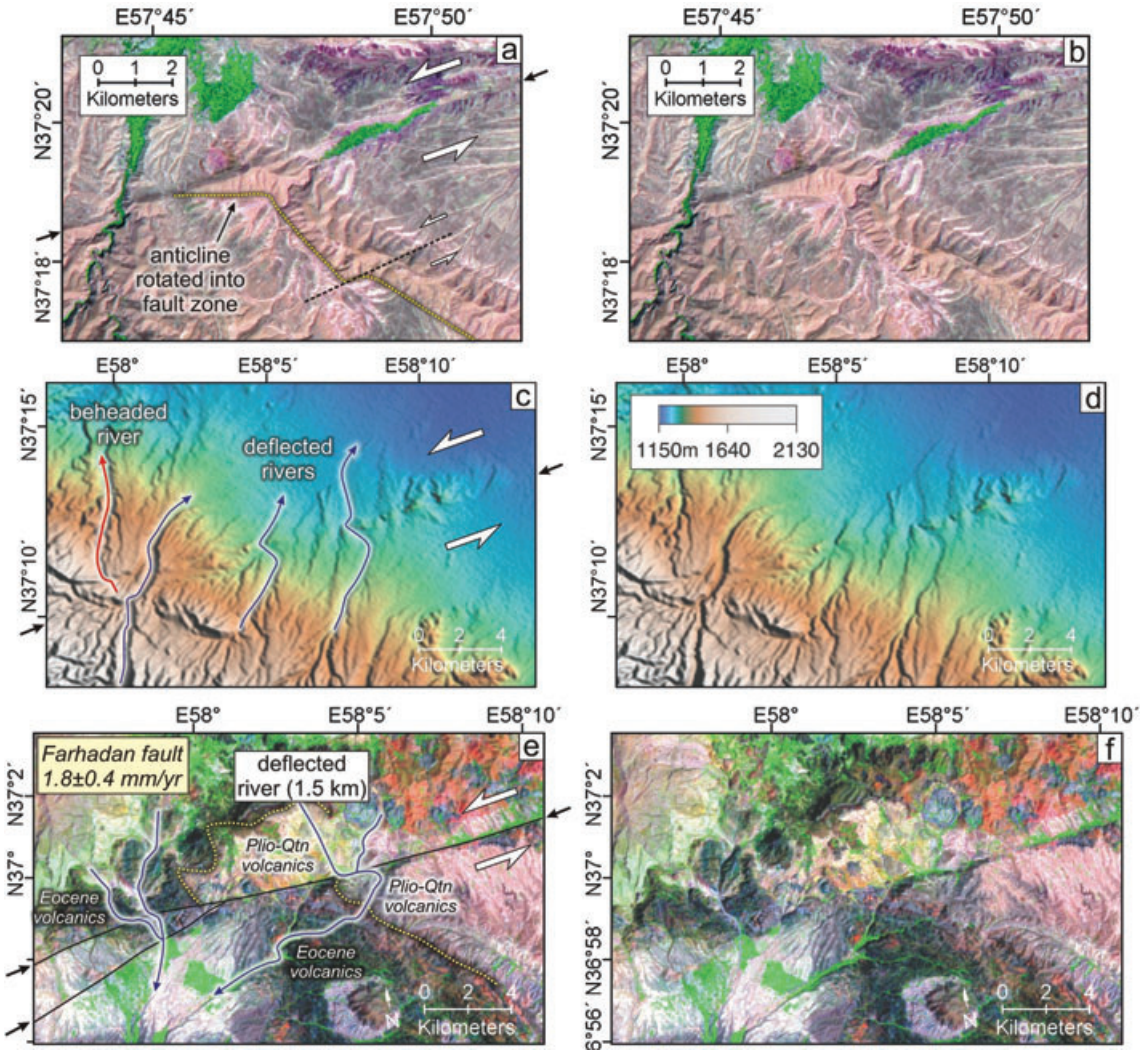

Figure 15. (a) Interpreted and (b) uninterpreted aster satellite images of the north side of the Alborz showing the northern-most left-lateral strike slip fault in Fig. 10. A Cretaceous limestone anticline (shown by a yellow dotted line along its southern margin) has been rotated into, and truncated across the fault zone which runs between the two heavy black arrows. (c) Interpreted and (d) uninterpreted images showing digital topography of the northern Alborz range front, SE of the region shown in (a)—see Fig. 10 for location. A strike-slip fault runs between the two black arrows and is visible in SRTM digital topography as a linear feature in the geomorphology. Two rivers (blue lines) have been deflected against the topographic slope (SW to NE), indicating 1 km of left-lateral slip during the Quaternary. This offset has also resulted in the beheading of a river, shown in red, across the fault. (e) Interpreted and (f) uninterpreted Aster satellite images of the southern-most left-lateral strike slip fault, referred to by Shabanian *et al.* (2009a) as the Farhadan fault (see Fig. 10), which cuts across a series of Cenozoic volcanics (between the black arrows; black lines show the fault trace). The dotted yellow line shows the boundary between Eocene(?) and Plio-Quaternary volcanics, which has been offset by up to 4 km. Blue lines show rivers that have been deflected against the overall westward drainage direction, indicating 1.5 km left-lateral motion.

regional shortening. A number of relatively small historical earthquakes have affected Herat city (849, 1102, and 1364—see Table 1, Fig. 21a, and Ambraseys & Bilham 2003, for further details). Wellman (1966) first documented the Herat (Harirud) fault, which is a major active right-lateral fault striking E–W along the Paropamisus mountains for more than 600 km (see also Tapponnier *et al.* 1981; Ruleman *et al.* 2007).

GPS velocities located in Iran either side of the western end of the Herat fault (ZABO and YAZT, see Fig. 1, and Masson *et al.* 2007), show little present-day shear across the fault zone, although they cannot accurately resolve slip rates <2 mm yr^{-1}. The geomorphology (Figs 22a and b) and historical seismicity indicate the Herat fault is an important active right-lateral strike-slip fault east of Herat city, which could therefore be slipping at a rate of 0–2 mm yr^{-1} without being resolved by existing and limited GPS data. West of Herat, the geomorphological expression of right-lateral strike-slip faulting becomes far less pronounced, although remnants of uplifted and abandoned fan surfaces along the southern edge of the mountain range suggests some shortening is accommodated across the range (Fig. 22c). Nevertheless, the morphology of the range front contrasts with that of Torbat-e-Jam only 40 km to the NW (Fig. 20 appearing less active based on its geomorphological expression; there is no clear topographic step along the range front (presumably the thrust fault is blind), there are significantly fewer and less extensive uplifted and incised alluvial fan surfaces overlying Neogene red beds, and the elevations of the range are much lower (by 800 m, Fig. 21b) than Torbat-e-Jam. Despite a relative lack of data with which to better constrain the active tectonics of Western Afghanistan, we suspect N–S shortening along the East Alborz, which accommodates the collision of Arabia and Eurasia,

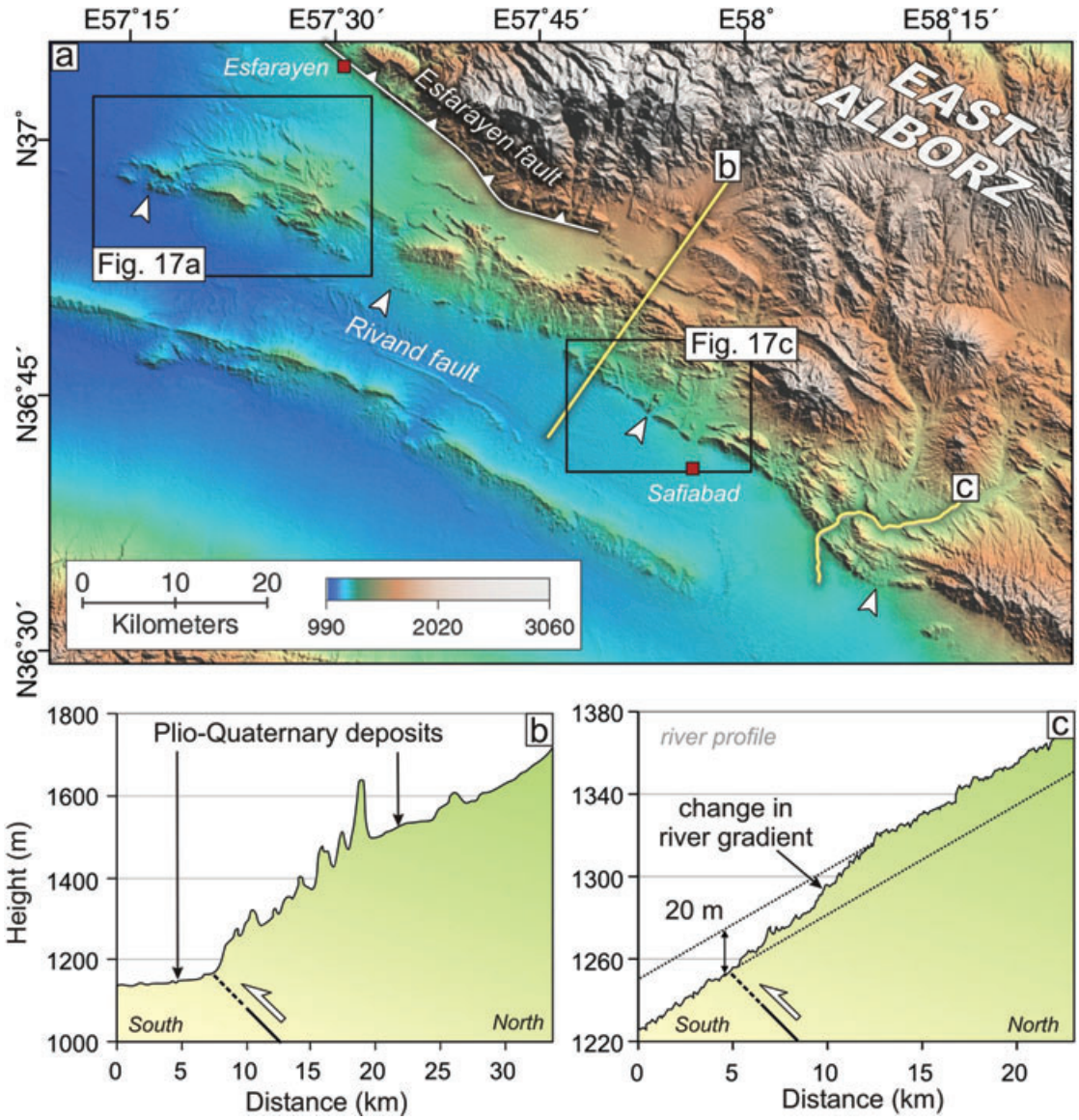

Figure 16. (a) SRTM digital topography of the region south of Esfarayen. The Esfarayen fault is shown by white line. The Rivand fault, which lies 15 km to the south, forms a low step in the topography, and is shown by white pointers. This step is highlighted by topographic profiles taken across the fault, the locations of which are shown by yellow lines. Black boxes show the locations of Figs. 17(a) and (c). (b) A Plio-Quaternary surface has been uplifted by the Rivand fault above the valley floor. (c) A river profile shows a change in gradient where it crosses the fault, indicating at least 20 m vertical offset during the Quaternary.

gradually dies out eastwards in the westernmost Paropamisus of NW Afghanistan. It is not clear what role the Herat fault plays in the regional kinematics, although it may be related to the westward motion (extrusion) of Central Afghanistan resulting from the India–Eurasia collision (Molnar & Tapponnier 1975; Tapponnier & Molnar 1976; Tapponnier *et al.* 1981, see Section 8 for more discussion).

6 ACTIVE TECTONICS OF THE SABZEVAR MOUNTAINS

Before discussing how regional shortening is distributed across NE Iran south of the Kopeh Dagh mountains, it is necessary to draw attention to the Sabzevar range, which lies 50–80 km south of the East Alborz mountains (Fig. 2). The Sabzevar (or Siah Kuh = 'black mountains') range consists of Cretaceous ophiolitic rocks obducted during the early stages of the Alpine Orogeny. The 200 km-long range reaches elevations of up to 2800 m and strikes WNW–ESE across NE Iran, subparallel to the East Alborz (Figs 2 and 23). A number of subparallel thrust faults occur on the southern side of the range, which may have been responsible for a destructive earthquake in 1052 (Ambraseys & Melville 1982; Fattahi *et al.* 2006, see also Table 1).

The active faulting of the Sabzevar range closely resembles that of the East Alborz near Esfarayen and Neyshabur, again showing a basinward migration of faulting (Figs 23a and b). The Sabzevar fault lies at the foot of the range, and has uplifted a band of red Neogene conglomerates, which form a low step in the topography (Figs 23c and d). Recent uplift across the Sabzevar fault has caused rivers to incise through the Neogene deposits, leaving a series of uplifted Quaternary fan surfaces (Fig. 23d). Using the OSL dating method, Fattahi *et al.* (2006) determined a 11 ± 2 kyr age for the

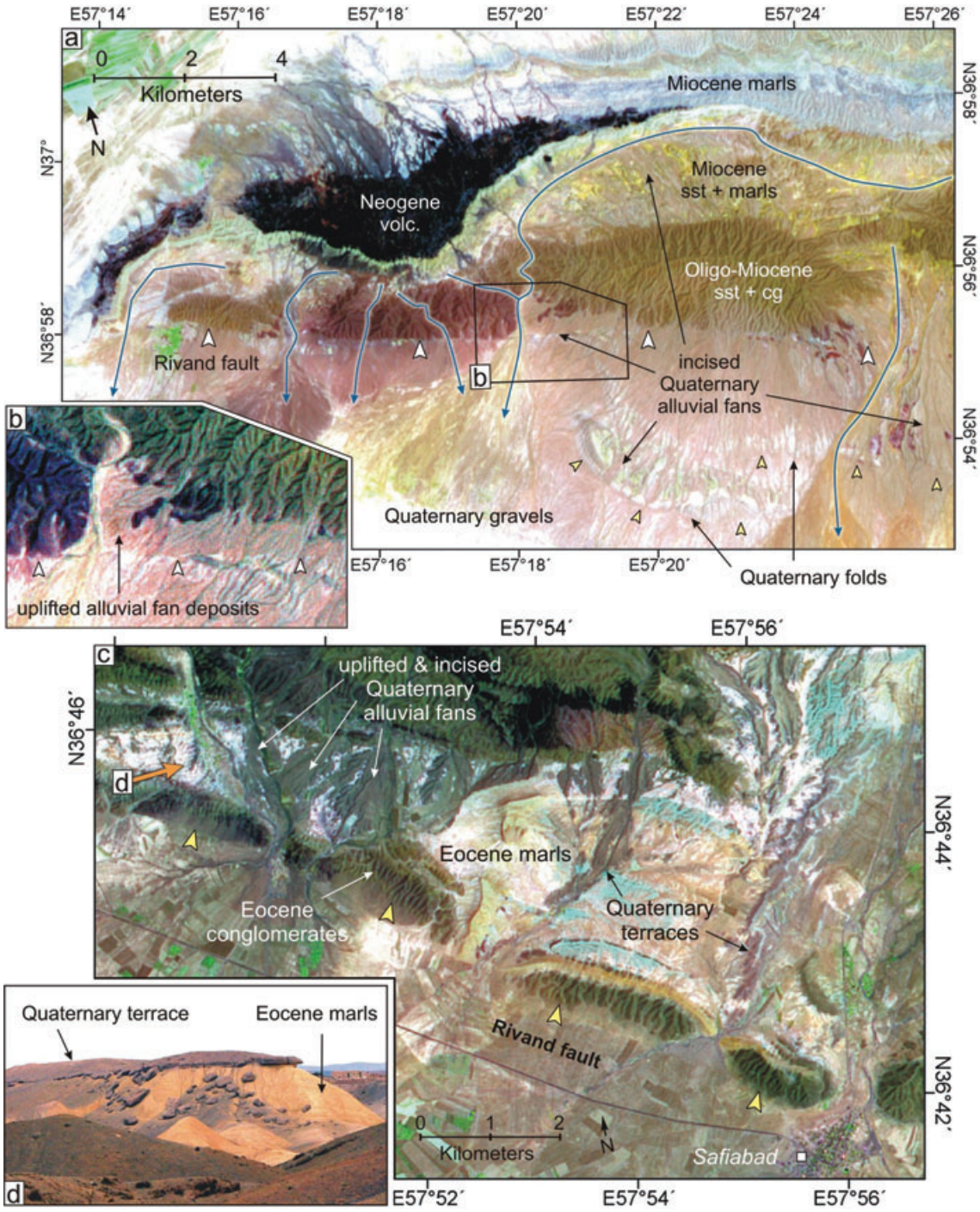

Figure 17. (a) Aster satellite image of the western end of the Rivand fault, which is marked by white pointers. Neogene sandstones, conglomerates, marls and volcanics have been uplifted by the fault into an E–W trending anticline. Young Quaternary folds occur south of the Rivand fault, and are marked by yellow pointers. Recent uplift has caused rivers (blue lines) to incise, leaving terraces across the fold. The black box shows the location of image (b), which shows alluvial fan deposits displaced across the Rivand fault. (c) Aster satellite image of the Rivand fault, marked by yellow pointers, near Safiabad village. Eocene conglomerates and marls have been uplifted to the north. Active river incision has resulted in the formation of river terraces and uplifted alluvial fans, which overly the Eocene marls. The orange arrow shows the location of the field photo in (d). This view is taken from 36°45.546′N 57°50.244′E, looking northeast. Quaternary conglomerates form resistant caps over the soft Eocene marls beneath. See Fig. 16a for locations of Figs. 17a and 17c.

lowest terrace, which had been uplifted by 9.5 ± 1 m by the fault (determined by kinematic GPS profiles), indicating an uplift rate of ∼1 mm yr^{-1}. The geomorphology of the Sabzevar fault contrasts significantly with the North Sabzevar fault, which lies 5–10 km to the north and shows little sign of Quaternary activity. Furthermore, the heights of abandoned alluvial fan surfaces at Sabzevar are similar to those at Neyshabur (where the uplift rate is also ∼1 mm yr^{-1}), and Esfarayen. This suggests similar uplift rates for all the range bounding thrust faults along the East Alborz.

OSL dating of a river terrace displaced across the Sabzevar fault indicates a Holocene shortening rate of 0.4–0.6 mm yr^{-1} (Fattahi *et al.* 2006, this assumes the fault cuts the entire crust;

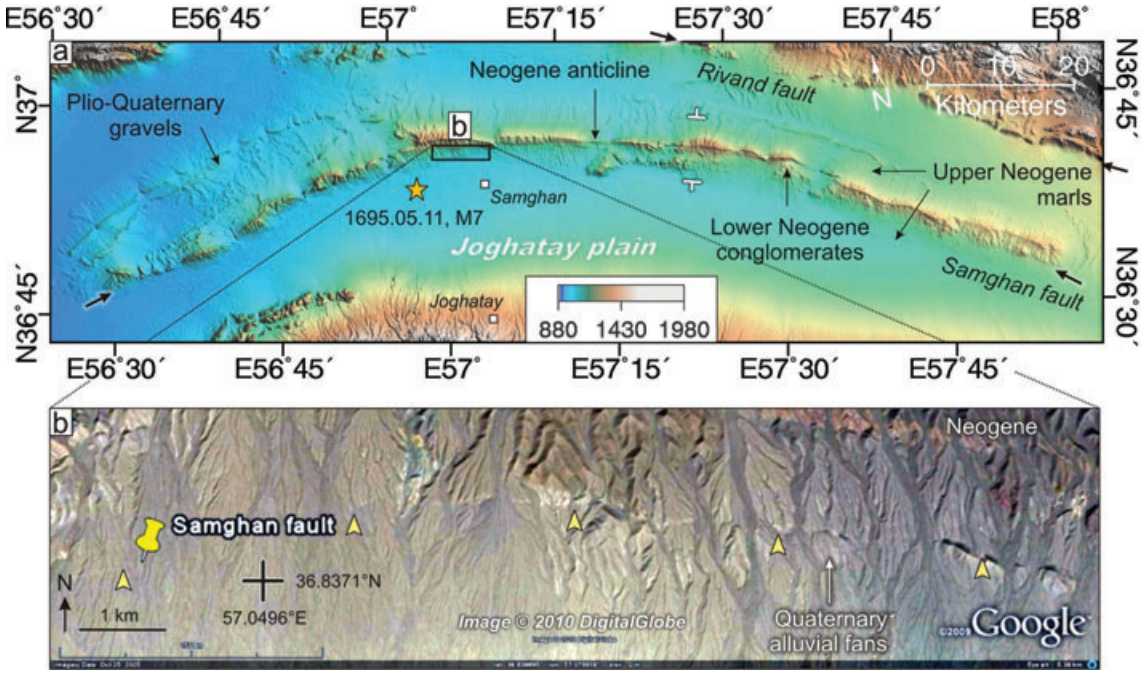

Figure 18. (a) Topographic map of the Joghatay region, south of the Rivand fault. A large Neogene fold strikes along the valley, forming a low ridge. A historical earthquake in 1695 (approximate location is shown by the star) may have occurred on this structure. (b) Quickbird satellite image (©2010 Google, ©2010 DigitalGlobe) showing the area north of Samghan village, a fault scarp is visible (marked by yellow pointers), cutting across Quaternary alluvial fans, which drain south of the ridge.

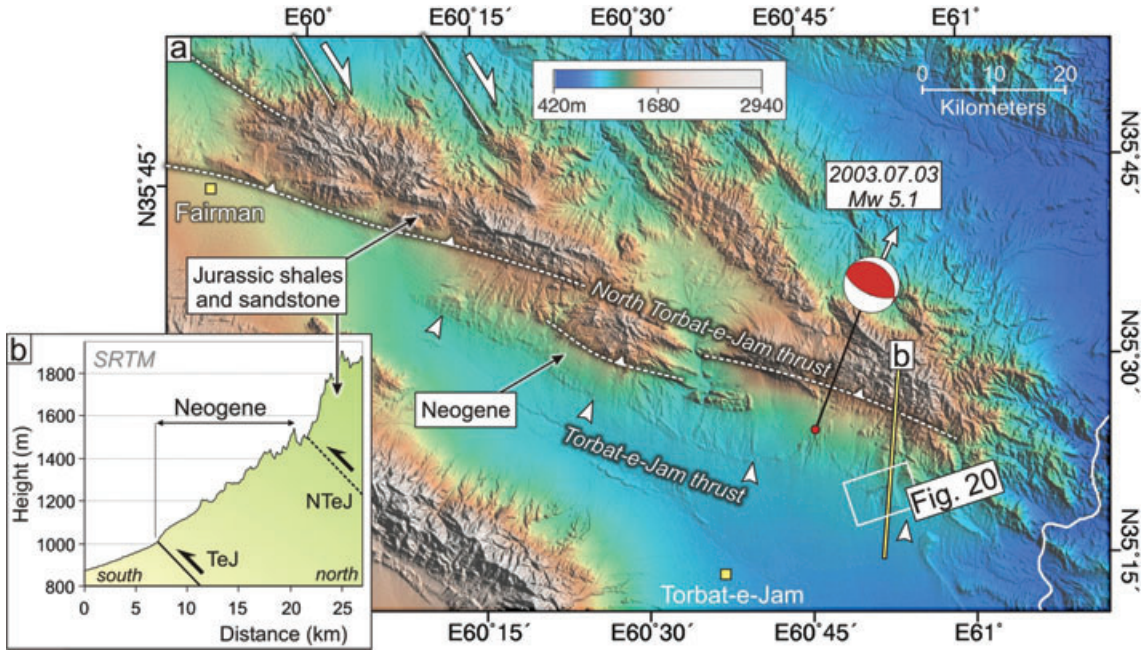

Figure 19. (a) Topographic image of the East Alborz mountains near Torbat-e-Jam, which lies near the Iran–Afghanistan border (curved white line). Older thrust faults, within the mountains, are shown by dotted white lines. South of these, the Torbat-e-Jam thrust (marked by white pointers) has produced a low step in the topography. The fault plane solution for a recent earthquake (2003.07.03) indicates NNE-shortening, perpendicular to the range front (slip vector is south relative to north and corresponds to slip on the north-dipping plane). Yellow line shows the location of a topographic profile across the range front shown in (b). A low Neogene step occurs at the base of the high topography, which has been uplifted by the Torbat-e-Jam thrust (TeJ). To the north, Jurassic shales and sandstones have been thrust over the Neogene deposits at the foot of the range by the North Torbat-e-Jam thrust (NTeJ), also shown by dashed white lines in (a).

Appendix S3). However, if the Sabzevar thrust forms a shallow splay from the North Sabzevar thrust, and extrudes Neogene material along a décollement which ramps to the surface along the present day trace of the Sabzevar fault (see Appendix S3), the horizontal shortening rate could be as much as 1 mm yr^{-1} (i.e. the value given by the fault slip rate). This view is supported by the relatively uniform 60° northward dip of the uplifted Neogene deposits along the range front (e.g. Fig. 6d), rather than horizontal

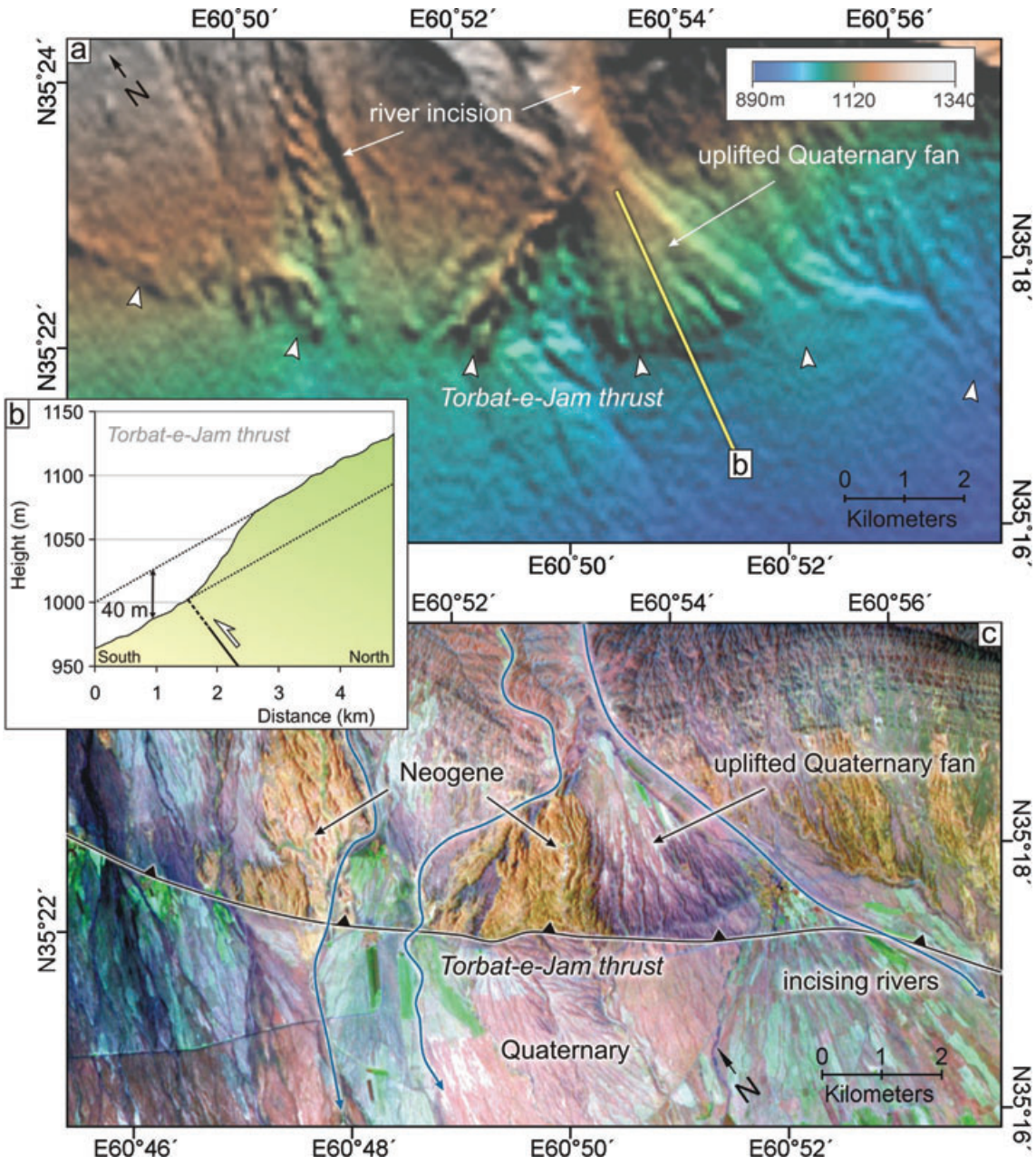

Figure 20. (a) Digital topography of the eastern Torbat-e-Jam thrust (see Fig. 19a for location), which forms a low step in the topography, marked by white arrows. (b) Topographic profile across an uplifted Quaternary fan, shown by the yellow line in (a), which has been displaced vertically by 40 m. (c) Aster satellite image of the region in (a) for comparison. 'Yellow' Neogene deposits have been thrust over 'purple' Quaternary gravels by the Torbat-e-Jam thrust (black line). Recent uplift has caused rivers (blue lines) to incise, leaving a series of river terraces and abandoned alluvial fans across the uplifted Neogene deposits.

bedding which would be expected if the fault did not sole into a décollement at depth.

7 ACTIVE TECTONICS OF THE KUH-E-SORKH MOUNTAINS

The Kuh-e-Sorkh mountains lie SE of the Sabzevar range, and consist of uplifted Eocene volcanics and Cretaceous ophiolitic material obducted at the start of the Alpine Orogeny. The range strikes broadly E–W for over 300 km, reaching elevations of 2800 m along its central portion, north of Kashmar city (Fig. 24a). Many earthquakes have occurred in the Kuh-e-Sorkh region (Fig. 2), which are mostly associated with deformation occurring along the south side of the range. The dominant active tectonic structure of the Kuh-e-Sorkh is the left-lateral Doruneh fault, which strikes for over 300 km along the southern range front and is one of the most distinctive tectonic features of NE Iran (Walker & Jackson 2004; Fattahi *et al.* 2007). It has been suggested the Doruneh fault accommodates left-lateral shear as a result of the clockwise rotation of rigid blocks bounding the range to the north and south (Walker & Jackson 2004). Thrust earthquakes which occur south of the Kuh-e-Sorkh (Fig. 2c) are related to shortening across a large Neogene fold (Fig. 24a). Although the majority of deformation appears to be concentrated along the southern part of the range, historical earthquakes are known to

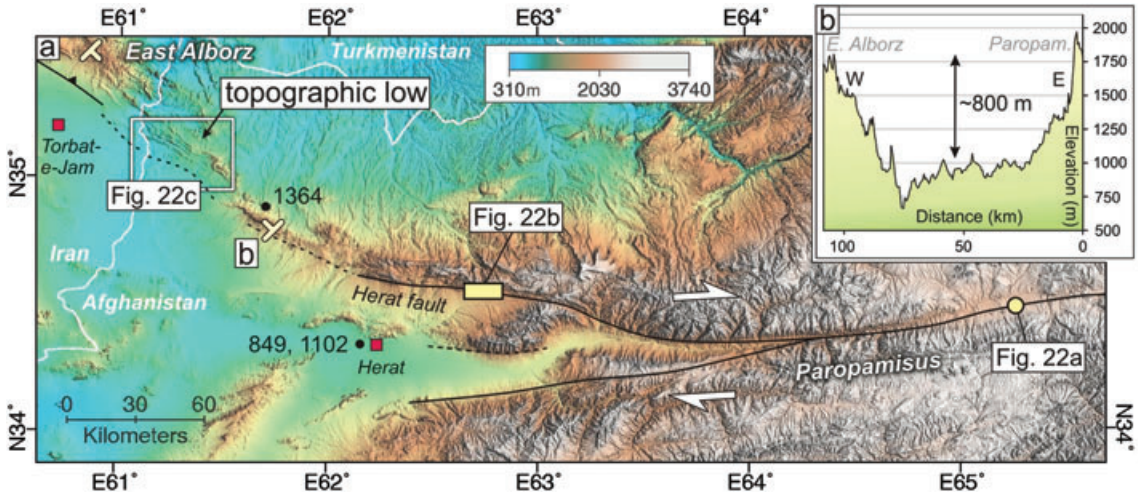

Figure 21. (a) Topographic map of the Iran–Afghanistan border region. A significant low in elevation occurs between the East Alborz and Paropamisus mountains near 61°E. Faults are shown in black. Approximate locations, and years, of large historical earthquakes are shown. Solid white line marks the border between Iran and Afghanistan. (b) SRTM topographic profile between the eastern end of the East Alborz and the western end of the Paropamisus mountains (see (a) for location of profile). The elevation decreases by 800 m between these two mountain ranges.

have affected the north side of the range near Torbat-e-Jam in 849 (M5–6?) and on 1918 March 24 (M5.9), and north of Kashmar on 1940 May 4 (M6.4), see Fig. 2. A more recent oblique thrust earthquake on 1971 May 26 (M_w 5.6) occurred in the central Kuh-e-Sorkh, and may be related to shortening either on the north or south side of the range (depending on which nodal plane corresponds to the fault plane). A possible aftershock on the 1972 December 1 (M_w 5.4) is located 30 km southwest of the 1971 event, and is related to left-lateral shear along the south side of the range, either on the Doruneh or a nearby parallel fault.

The high elevation of the Kuh-e-Sorkh mountains, particularly along the northern margin, suggests significant N–S shortening is also accommodated across this range. Figs 24(b)–(d) show examples from the northern side of the Kuh-e-Sorkh where evidence of recent uplift on active thrust faults bounding the range front is visible in the geomorphology. East of Torbat-e-Heydarieh (Fig. 24a), the Kuh-e-Sorkh range splits into two parallel branches. Clear expression of the Jangal thrust system in the Quaternary geomorphology, which may have ruptured in a large earthquake on 21st October 1336 (Table 1), suggests significant N–S shortening is accommodated across the southern branch of the range (Fig. 24a, for further discussion, see Walker & Jackson 2004). Shortening also occurs on north-dipping thrust faults bounding the southern margin of the northern branch. Fig. 24(e) shows a section of the range front where uplift on an older fault within the mountains (dotted white line in Fig. 24e) has thrust Palaeozoic rocks over Neogene deposits to the south. Recent migration of faulting to the south has thrust these Neogene deposits over Holocene flood plain deposits. Rivers draining southwards across the hangingwall have incised, leaving a series of uplifted and abandoned alluvial fan surfaces (Fig. 24e). Therefore, the geomorphology of this section of the Kuh-e-Sorkh mountains resembles that of the East Alborz and Sabzevar ranges, where a similar Neogene step is present along the range front.

8 DISCUSSION

In this section, we summarize the pattern of faulting for the Kopeh Dagh, East Alborz, Sabzevar and Kuh-e-Sorkh mountains, and then discuss the active tectonics of this region in relation to Arabia–Eurasia shortening.

8.1 Pattern of faulting

Shortening across NE Iran north of the East Alborz is accommodated in the Kopeh Dagh mountains. The fault kinematics varies dramatically along strike of this range (see Hollingsworth *et al.* 2008, and Fig. 25). East of 59°E shortening occurs by oblique slip on range-bounding thrust faults. Between 57–59°E anticlockwise rotation of right-lateral strike-slip faults which cut obliquely across the range appear to accommodate across-strike shortening and along-strike extension. West of 57°E, N–S shortening is accommodated by the westward extrusion of the Kopeh Dagh between transpressional fault systems in the East Alborz (Khazaar and Shahrud fault zone) and Kopeh Dagh-Balkan ranges (Ashkabad fault zone), see Fig. 25. The westward motion of the West Kopeh Dagh relative to the East Kopeh Dagh is therefore accommodated by along-strike elongation within the Central Kopeh Dagh (Hollingsworth *et al.* 2008).

Shortening south of the Kopeh Dagh is accommodated on active thrust faults which bound the south side of the East Alborz (east of 57°E) and Sabzevar ranges, and the north side of the Kuh-e-Sorkh range. Left- and right-lateral strike slip faults on the north side of the East Alborz also accommodate some of this shortening (Fig. 25). Basinward migration of faulting has resulted in a series of subparallel thrust faults along the various range fronts. Present day shortening is concentrated on the southernmost and youngest of these faults, which have uplifted Neogene deposits, forming a low step along the edge of the topography. River incision across this zone has resulted in the abandonment of alluvial fan surfaces, which overlie the uplifted and folded Neogene. Optically stimulated luminescence dating of displaced Quaternary fan surfaces on the Neyshabur and North Neyshabur fault, as well as the Sabzevar thrust to the south, indicate low rates of shortening (<2 mm yr^{-1}) across the East Alborz and Sabzevar mountain ranges. Similar rates are likely near Esfarayen, based on the correlation of regional terrace heights. Nevertheless, a more comprehensive

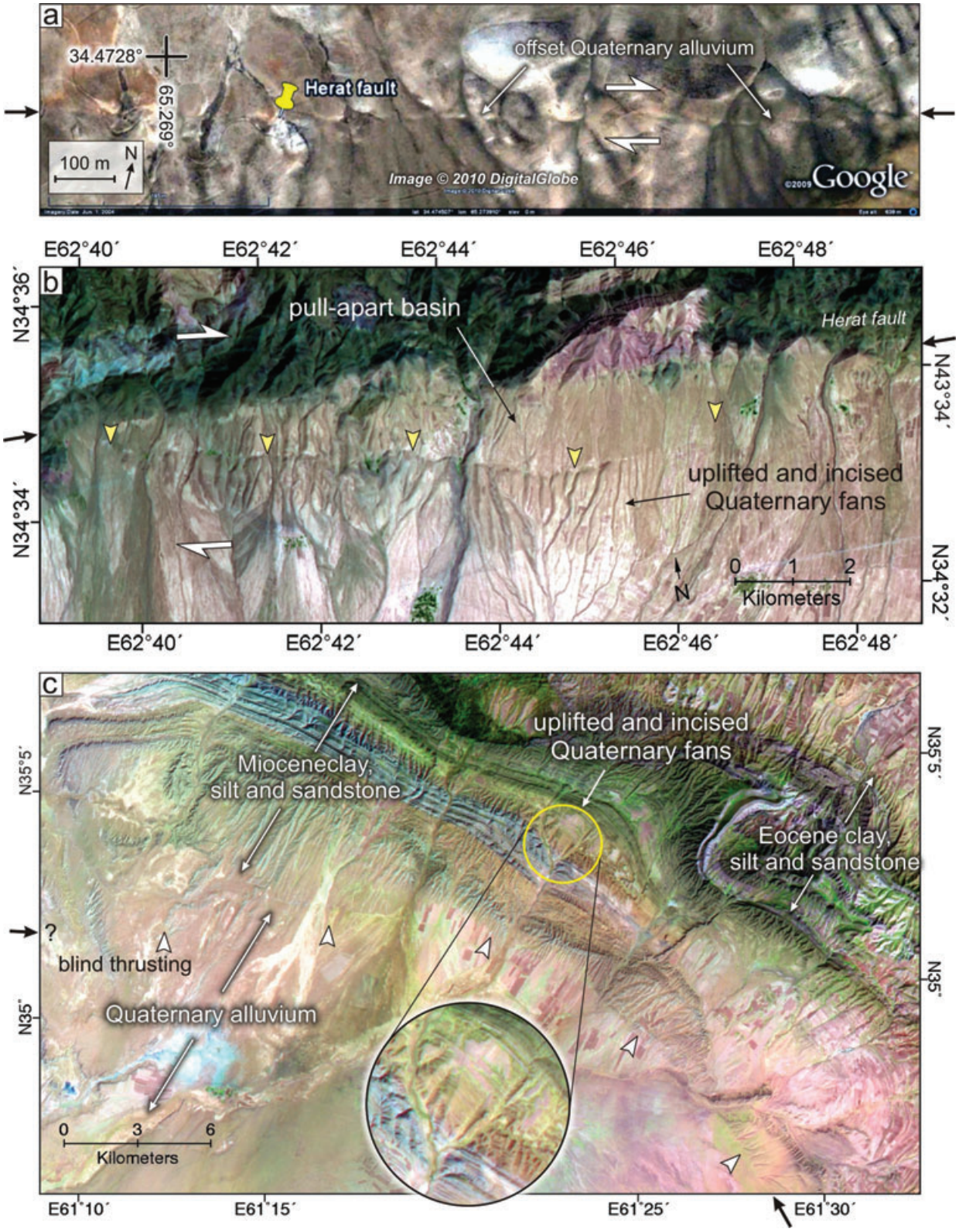

Figure 22. (a) Quickbird satellite image (©2010 Google, ©2010 DigitalGlobe) of the right-lateral Herat fault, which cuts linearly across a series of Quaternary fans (between the black arrows), deflecting and beheading drainage systems across the fault. (b) Aster satellite image of the Herat fault, which steps south of the range front (marked by yellow pointers), forming a small pull-apart basin. Quaternary fan deposits have been uplifted and incised (possibly as a result of footwall uplift), indicating recent activity on the Herat fault. (c) Aster satellite image of the southern East Alborz-Paropamisus range front near the Iran–Afghanistan border. Miocene terrestrial deposits have been uplifted along the range front, although the absence of a clear fault scarp suggests thrust faulting is blind (the approximate location of the fault trace at depth is shown by the white pointers). Circular inset shows remnant Quaternary alluvial fan surfaces which became abandoned as rivers incised in response to uplift. For locations see Fig. 21.

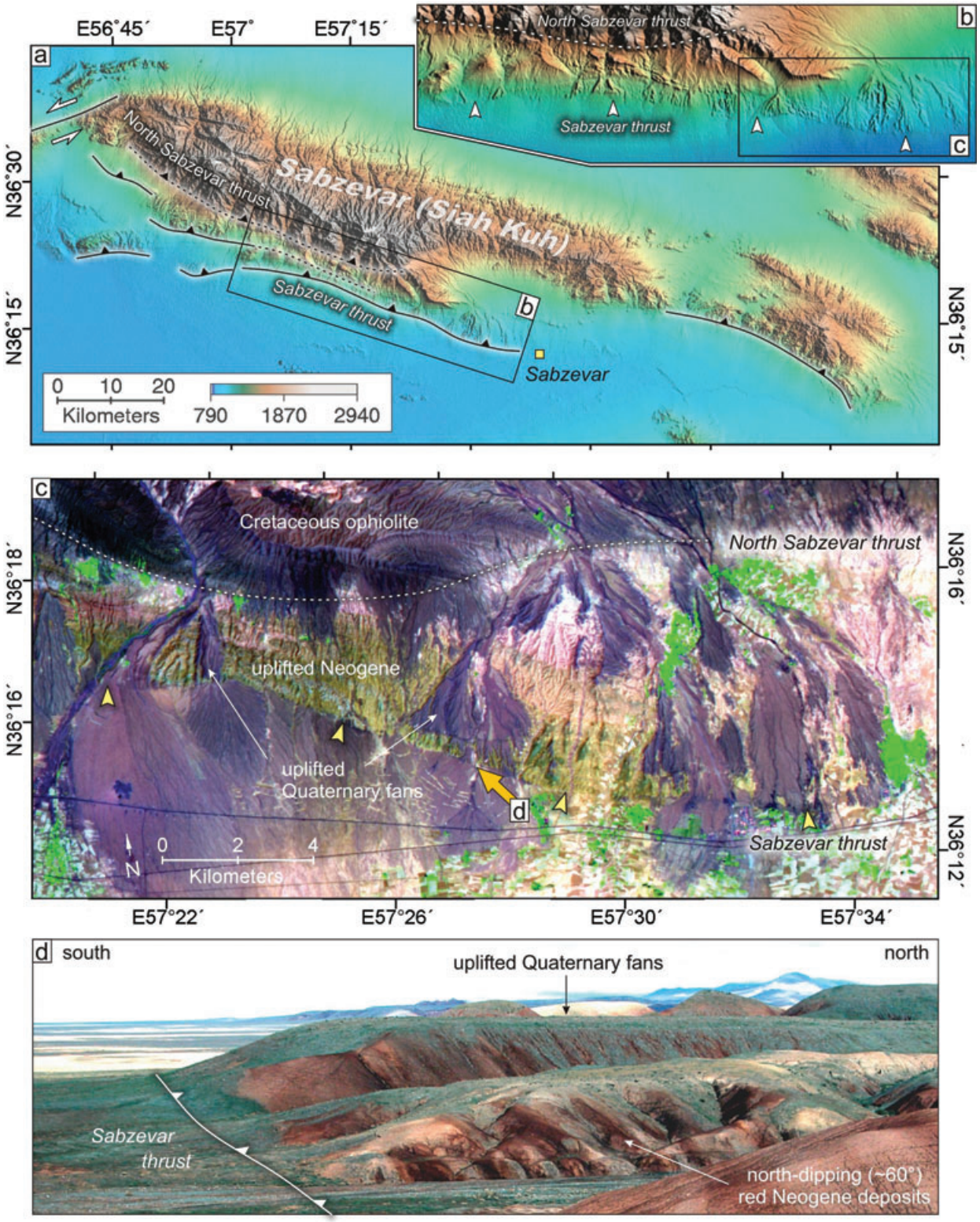

Figure 23. (a) Topographic map showing the Sabzevar (Siah Kuh) mountain range (see Fig. 2 for location). Faults are shown by black lines. (b) Close-up of the Sabzevar thrust (marked by white pointers for clarity). The North Sabzevar thrust lies 5 km north of the Sabzevar thrust, within the mountains. (c) ASTER satellite image of the eastern end of the Sabzevar thrust. Dashed white line shows the North Sabzevar thrust which thrusts Cretaceous ophiolite material over Neogene deposits. Yellow pointers mark the Sabzevar thrust, which thrusts Neogene over Quaternary flood plain deposits. 'Purple' areas north of the Sabzevar thrust are Quaternary alluvial fans which have been uplifted and incised by rivers draining south of the mountains. Orange arrow shows the location of the field photo shown in (d). This view is taken from 36°14.321′N 57°27.902′E looking northwest at the Sabzevar fault scarp. Uplifted Quaternary deposits overlie 60° north-dipping red Neogene deposits.

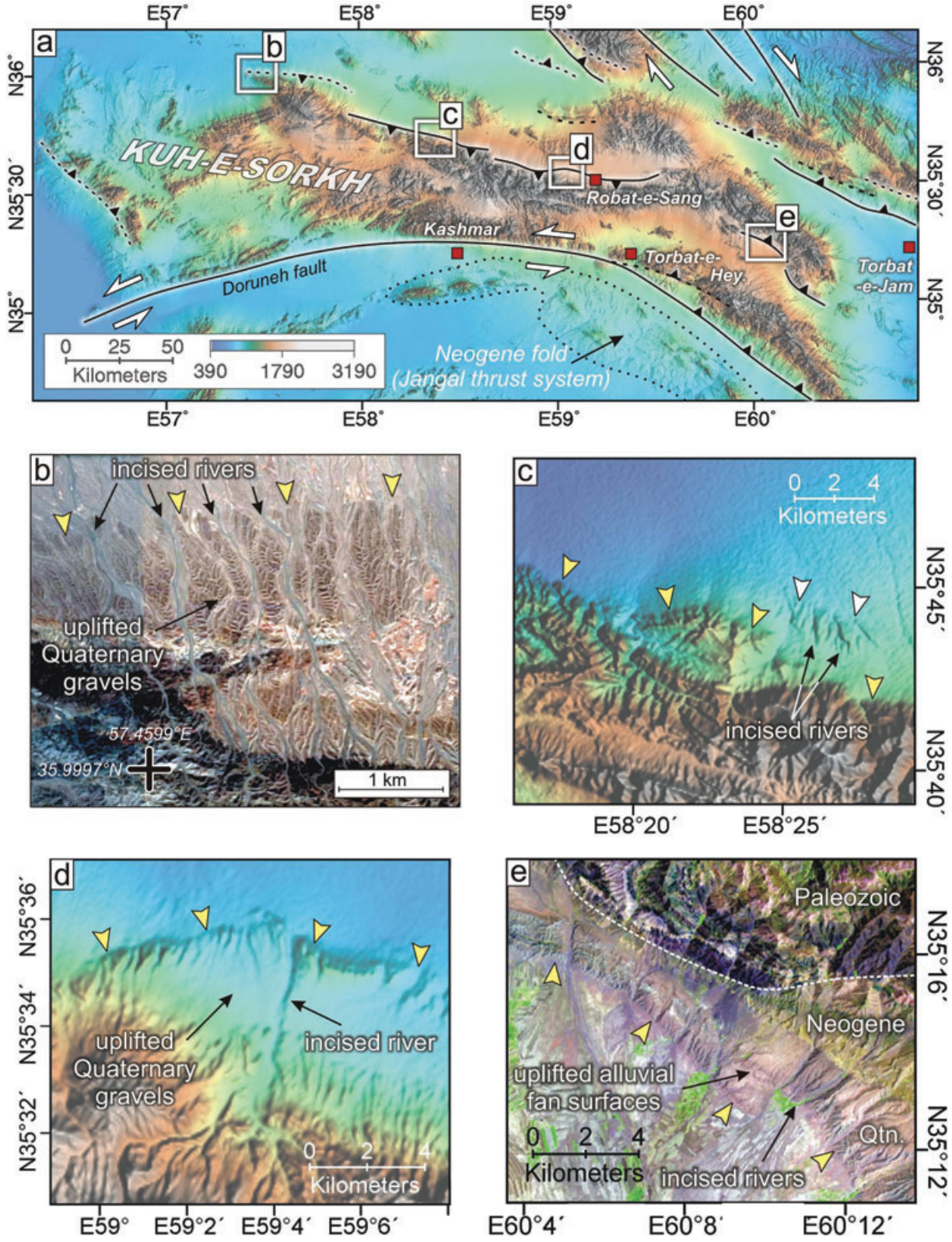

Figure 24. (a) Topographic map showing the Kuh-e-Sorkh mountain range (see Fig. 2 for location and associated seismicity). Faults are shown by black lines. Examples of Quaternary uplift on range bounding thrust faults from the northern Kuh-e-Sorkh are shown in (b) to (d). Yellow and white pointers highlight the locations of active thrusts, which are probably blind in examples (b) and (c). These thrust faults are all south-dipping and recent uplift in the hangingwall has caused rivers to incise though Quaternary flood plain deposits bounding the range. (e) Example of an active thrust fault from the northern branch of the eastern Kuh-e-Sorkh. Uplift on a north-dipping thrust fault which runs along the southern margin range has resulted in river incision and the formation of abandoned Quaternary alluvial fan surfaces. Evidence for the southward migration of thrust faulting is indicated by the formation of a low Neogene step at the foot of the range (see text for details). Qtn, Quaternary.

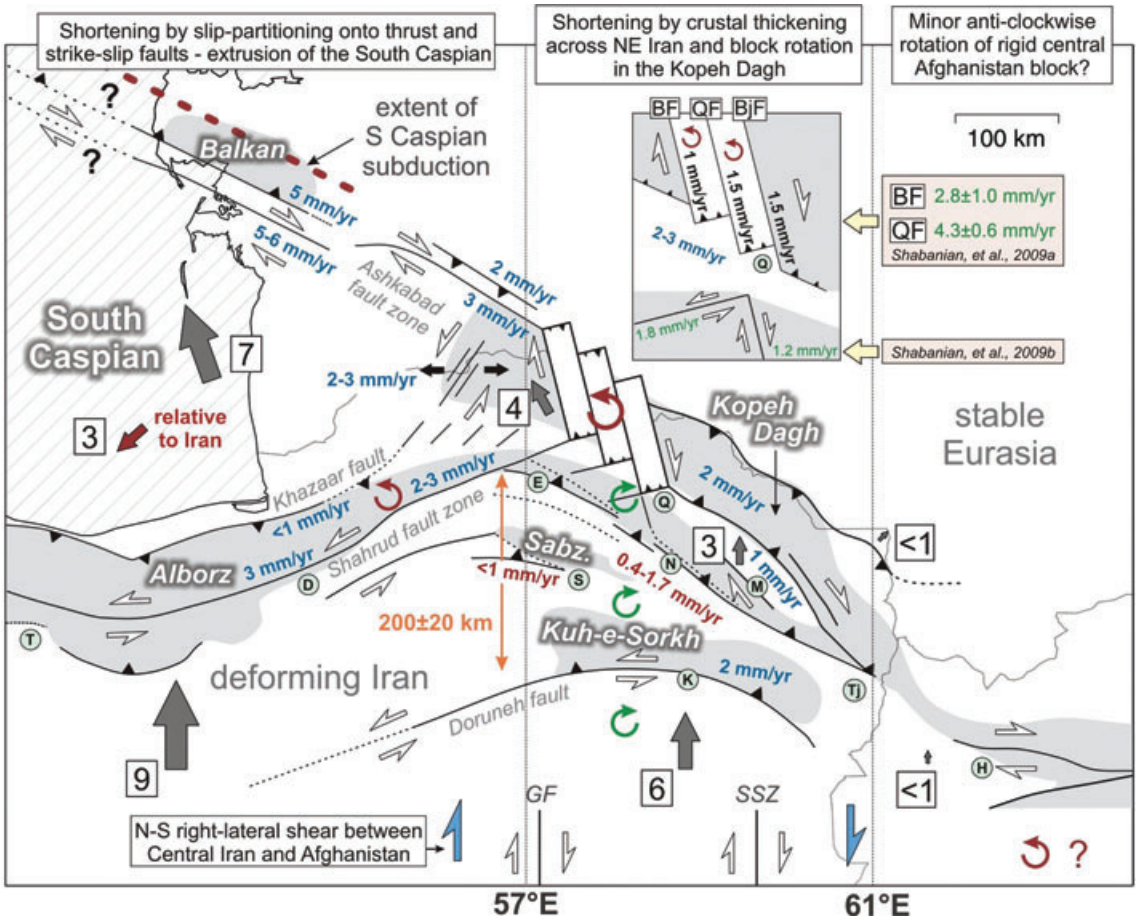

Figure 25. (a) Simplified summary tectonic map of NE Iran modified from (Hollingsworth *et al.* 2008). Faults are shown in black. Grey areas are various mountain ranges in NE Iran. Major cities are shown by pale green circles (see abbreviations below). Anticlockwise rotating blocks of the Central Kopeh Dagh are shown schematically both in the main figure and in the inset (Hollingsworth *et al.* 2006). Grey arrows and their associated values show approximate northward velocities across NE Iran, relative to Eurasia, and the red arrow shows the South Caspian Sea relative to Central Iran, based on the GPS data of (Masson *et al.* 2007). Orange double-headed arrow indicates the amount of oroclinal bending (assuming an original E–W strike) which has occurred in the East Alborz range (equivalent to 200 ± 20 km N–S shortening). Dotted red line shows the maximum northern extent of the NW Kopeh Dagh-South Caspian block as it underthusts the Balkan region (Eurasia)—see also Hollingsworth *et al.* (2008). Fault slip rates in blue (horizontal shortening rates for thrust faults) are estimates extrapolated from the coarse distribution of GPS velocities across NE Iran (Masson *et al.* 2007; Hollingsworth *et al.* 2008). Shortening rates in red, at Sabzevar and Neyshabur, have been determined from OSL dating of displaced geomorphology. Slip rates in green are Quaternary estimates from Shabanian *et al.* (2009a,b). Green (clockwise) and red (anticlockwise) arrows indicate the direction of rotation of the East Alborz it becomes progressively deflected away from its original E–W strike. N–S shear across East Iran (blue arrows) is accommodated on the Gowk-Nayband Fault System (GNFS) and Sistan Suture Zones (SSZ) N–S strike-slip fault systems, shown schematically in this figure. North of these faults, N–S right-lateral shear is accommodated by clockwise rotation of rigid blocks bounding either side of the Kuh-e-Sorkh. Walker & Jackson (2004) suggest that left-lateral motion occurs between these blocks as they rotate past each other, which is accommodated by the left-lateral Doruneh fault. The tectonics of the East Alborz range change dramatically from partitioning of oblique slip west of 57°E, to predominantly thrust faulting east of 57°E. Deformation dies away near the Afghanistan border at 61°E, although minor present-day right-lateral slip occurs on the Herat fault, which may be related to an anticlockwise rotation of Central Afghanistan. Shortening across the Kopeh Dagh is accommodated by oblique slip on range-bounding thrust faults east of 59°E, anticlockwise rotation of right-lateral strike-slip faults which cut obliquely across the range between 57–59°E, and westward extrusion of the West Kopeh Dagh block between transpressional fault systems in the East Alborz and Kopeh Dagh-Balkan ranges. Abbreviations: T, Tehran; D, Damghan; E, Esfarayen; S, Sabzevar; A, Ashkabad; Q, Quchan; N, Neyshabur; K, Kashmar; M, Mashad; Tj, Torbat-e-Jam; H, Herat; BF, Baghan fault; QF, Quchan fault; and BjF, Bajgiran fault.

dating program is required to provide a more robust picture of fault slip rates along the East Alborz range front.

No significant strike-slip component is visible in the Quaternary geomorphology along the southern East Alborz and Sabzevar range fronts, indicating NNE-directed shortening occurs perpendicular to the ranges. This is consistent with the slip vectors of recent thrust earthquakes in the East Alborz near Esfarayen and Torbat-e-Jam (Fig. 2). Nevertheless, a small amount of right-lateral motion is accommodated by the Shandiz fault on the north side of the Binalud mountains, and may indicate a shortening direction which is slightly oblique to the range at this longitude. This is consistent with the N-directed slip vectors of two earthquakes which occurred in the SE Kopeh Dagh, north of Mashad, on 1968 November 15 and 1985 August 16 (Fig. 2). The northern side of the East Alborz, west of 58.5°E, is truncated by a series of left-lateral strike-slip faults, which are conjugate to the right-lateral faults of the Central Kopeh Dagh, and accommodate along-strike elongation of the range (Fig. 25).

The elevation of the East Alborz mountains decreases significantly at the Iran–Afghanistan border, where N–S shortening

associated with the Arabia–Eurasia collision dies out. The Paropamisus mountains lie eastward of the East Alborz, and strike E–W across northern Afghanistan (Fig. 25). A small amount of active deformation occurs in the Paropamisus on the E–W right-lateral Herat fault, which runs for >600 km between Herat and Kabul.

8.2 Kinematics of East Alborz deformation

Velocities of GPS stations across NE Iran indicate an eastward decrease in N–S shortening across the region from 9 mm yr^{-1} at SEMN, to 6 mm yr^{-1} at KASH (Fig. 2), and 2 mm yr^{-1} at ZABO near the Iran–Afghanistan border in East Iran (east of the Lut block, Fig. 1a).

The Kopeh Dagh mountains accommodate a significant amount of this motion, by a combination of slip-partitioning in the NW, thrust faulting in the SE, and anticlockwise block rotation in the Central Kopeh Dagh (Hollingsworth *et al.* 2006, 2008)—see Fig. 25. However, active thrust faulting in the East Alborz, Sabzevar and Kuh-e-Sorkh mountain ranges indicates that shortening also occurs south of the Kopeh Dagh. At the longitude of Neyshabur, the East Alborz range contribute 0.4–1.7 mm yr^{-1} to the regional shortening, based on a relatively small set of OSL ages for two displaced Quaternary alluvial fans (Fig. 25). This is broadly consistent with a 3 $\pm$ 2 mm yr^{-1} difference in northward velocity between GPS stations at Mashad (MSHN) and Kashmar (KASH), which lie north and south of the range, respectively (Figs 1 and 25, see also Masson *et al.* 2007). However, this higher GPS shortening estimate also includes a component of shortening which is accommodated across the Kuh-e-Sorkh mountains south of the East Alborz, and is likely to be in the range of 2.3 $\pm$ 2.3 mm yr^{-1} (this value accounts for the range of GPS shortening estimates between Kashmar and Mashad minus the OSL shortening estimates across the East Alborz; see also Fig. 25). Such a shortening rate is also consistent with the similar 3 km elevations of the East Alborz and Kuh-e-Sorkh ranges at the longitude of Kashmar and Neyshabur (59°E). Further west, the Sabzevar range also contributes ∼1 mm yr^{-1} to the regional shortening. Therefore, of the 6 mm yr^{-1} N–S shortening which occurs between Kashmar and Turkmenistan (i.e. stable Eurasia), roughly half is accommodated in the Kopeh Dagh, and the other half in the various subparallel mountain ranges to the south (see also Masson *et al.* 2007). The current lack of well-resolved dense continuous GPS measurements, detailed Quaternary dating fault slip rate studies and knowledge of the geometry of active faults at depth throughout NE Iran prevents a more accurate and precise strain field from being determined. Furthermore, although Jackson & McKenzie (1988) and Masson *et al.* (2005) found that 50–100 per cent of the deformation in NE Iran is accommodated seismically, presumably on structures such as those detailed in this study, a certain amount of shortening must also be accommodated by distributed aseismic deformation to produce the folded geology that we see across the region. Although beyond the scope of this study, future detailed geological cross sections across all the structures in NE Iran will provide valuable constraints on the amount of aseismic deformation accommodated across this region over geological timescales. Present-day slip rates estimated for the major fault systems across NE Iran, based on the GPS velocity field (e.g. Hollingsworth *et al.* 2008) may therefore overestimate the real rates by as much as 50 per cent. However, due to the relatively low rates of shortening (typically <1 mm yr^{-1}) across these faults, such an overestimate will not be resolvable within the error of the determined rates. Despite the broad range of error in the rates of deformation presented in this study, they represent the first attempt at constraining fault slip rates in this region, and understanding how these fault systems accommodate regional shortening resulting from the Arabia–Eurasia collision.

The change in tectonics across the Kopeh Dagh (i.e. extrusion in the NW, anticlockwise block rotation in the Central, and N–S shortening in the SE) is also reflected in East Alborz mountains to the south. West of 57°E, N–S shortening is accommodated by slip-partitioning onto thrust faults north of the range (Khazaar fault) and left-lateral faults on the south side of the range (Shahrud fault system)—see Fig. 25 and Hollingsworth *et al.* (2008). East of 57°E, NNE-shortening occurs on thrust faults bounding the south side of the range, with only minor partitioning onto strike-slip faults on the north side. It is in this region that the highest elevations of the East Alborz occur (3 km).

The topography of the East Alborz mountains, seismicity and the general northward velocity of GPS stations across NE Iran all significantly decrease east of Torbat-e-Jam, near the Iran–Afghanistan border, suggesting that virtually all of the shortening between Arabia and Eurasia has been accommodated in NE Iran, and does not continue eastwards into Afghanistan. Therefore, an important structural change must occur in the Iran–Afghanistan border region (61°E): to the west, deformation in NE Iran accommodates Arabia–Eurasia collision by shortening predominantly on thrust faults in the Kopeh Dagh, Alborz, Sabzevar and Kuh-e-Sorkh ranges; to the east, minor E–W right-lateral shear occurs across much of northern Afghanistan. It is not clear what the role of the Herat fault is within the present day kinematics of the region, as E–W right-lateral slip cannot easily accommodate N–S regional shortening. Nevertheless, slip on the Herat fault may be associated with the India–Eurasia collision, with perhaps minor westward movement of Afghanistan, relative to Eurasia (see also Molnar & Tapponnier 1975; Tapponnier & Molnar 1976; Tapponnier *et al.* 1981). However, the presence of the Herat fault might also be explained by minor anticlockwise rotation of the relatively rigid (and aseismic) Central Afghanistan block about a vertical axis, relative to stable Eurasia to the north (Treloar & Izatt 1993). Not only does the latter explanation avoid the space problems encountered if Afghanistan extrudes westward into Iran, but it is also consistent with sparse palaeomagnetic data from East Central Afghanistan (33.25°N E62.12°E) which indicates ∼5° anticlockwise rotation since the Oligo-Eocene (23–56 Ma) and South Central Afghanistan (31.55°N E65.49°E) which indicates ∼40° anticlockwise rotation since the Lower Cretaceous (Barremian period; 125-130 Ma—for further details, see Krumsiek 1976).

The kinematic model for NE Iran presented here builds on the earlier studies of Jackson *et al.* (2002) and Hollingsworth *et al.* (2008), and incorporates kinematic information on the Kopeh Dagh from Hollingsworth *et al.* (2006) and Shabanian *et al.* (2009a). A slightly different kinematic model for the this region is presented by Shabanian *et al.* (2009b) which does not involve anticlockwise rotation of blocks in the Central Kopeh Dagh, but instead features a simple translation of material across both the Kopeh Dagh and Alborz-Binalud ranges. Key observations can be used to argue for each model, but ultimately we suspect along-strike elongation by block rotation plays some kind of role in accommodating E–W extension in the Central Kopeh Dagh, due to the linear range front across the northern Central Kopeh Dagh (as opposed to an offset range front predicted by a translation model), as well as anticlockwise rotation of anticlines visible in satellite images across the Central Kopeh Dagh, and which is not seen in the Alborz-Binalud (Hollingsworth *et al.* 2006). Furthermore, the translation model of Shabanian *et al.*

(2009a) relies on unpublished GPS velocities for NE Iran, which, in places, appear inconsistent with earlier GPS studies of Vernant *et al.* (2004b) and Masson *et al.* (2007), and new velocities from the denser network of GPS stations deployed throughout NE Iran (A. Walpersdorf, personal communication, 2009). For further discussion on these different models, see Hollingsworth *et al.* (2009), and references therein. Nevertheless, future more comprehensive Quaternary slip rate studies, which make use of multiple dating methods, and dense continuous GPS velocities, will undoubtedly shed more light on the kinematics of the NE Iran region and further refine both the model presented here, and that of Shabanian *et al.* (2009b).

The East Alborz curve dramatically across NE Iran, deviating from their general E–W strike by 200 ± 20 km near 57°E (estimated from their topographic expression, Fig. 25). If this oroclinal bending began to accumulate with the uplift of the Kopeh Dagh foreland basin in the early-to-middle Oligocene (post 30 Ma, see Section 2.2), and assuming the original strike of the range was E–W, it may record the total amount of shortening to have occurred across the East Alborz and Kopeh Dagh in NE Iran since this time (Fig. 26). Although little is known regarding the initial geometry of the Alborz, it might be reasonable to assume an early E–W-trending Alborz range, since this is consistent with the general E–W strike of the PTS across north central Iran and the Paropamisus range in Afghanistan (see Şengör 1987). Also the Talysh, Alborz and East Alborz mountains form a continuous range around the southern side of the South Caspian block which might have been produced by the rigid Central Iranian block colliding with and engulfing the smaller rigid South Caspian block, and the Talysh and East Alborz mountain ranges progressively wrapping around the Southern Caspian (e.g. Allen *et al.* 2003). Furthermore, because ≥75 km N–S shortening has occurred in the Kopeh Dagh since the East Alborz formed (Lyberis & Manby 1999; Hollingsworth *et al.* 2006), if the latter were uplifted as an arcuate range to begin with then a similar 75 km of shortening must have been accommodated in the South Caspian, either by folding or subduction beneath the Apsheron-Balkan Sill, to balance the shortening in the Kopeh Dagh. If the total shortening since Kopeh Dagh uplift is less in the South Caspian compared with the Kopeh Dagh, then the East Alborz would have been dragged northwards during this time. Estimates vary for the onset of subduction in the South Caspian, ranging from 1.8 Ma (Ritz *et al.* 2006), 3.4 Ma (Devlin *et al.* 1999), 5.5 Ma (Allen *et al.* 2002) and 10–15 Ma (Hollingsworth *et al.* 2008). Nevertheless, if subduction is ≤5.5 Ma (the 10–15 Ma estimate of Hollingsworth *et al.* (2008) is a loosely constrained upper estimate), and the South Caspian has been moving NNW during this time at 7 mm yr^{-1}, relative to Eurasia (Masson *et al.* 2007; Hollingsworth *et al.* 2008), then this would account for less than half of the total N–S shortening observed in the Kopeh Dagh (i.e. ≤35 km), therefore implying that the East Alborz must have been dragged northwards during the Late Cenozoic, or that significant shortening must have occurred within the South Caspian block. However, it should be noted that the similar northward velocity of GPS stations (relative to Eurasia) on the north side of the Central and East Alborz (Masson *et al.* 2007, Walpersdorf, pers. comm. 2009) indicate that, at the present day, the East Alborz are not being dragged northwards. Therefore, if deflection of the East Alborz has occurred, it is likely to have begun at the beginning of Kopeh Dagh uplift (post early-to-middle Oligocene, <30 Ma) and ended sometime in the Mio-Pliocene, presumably when subduction of the South Caspian began. Despite insufficient data to conclusively show oroclinal bending of the East Alborz has occurred during the Late Cenozoic, this new model provides a new and consistent interpretation for the tectonic evolution of the East Alborz, which bears further testing.

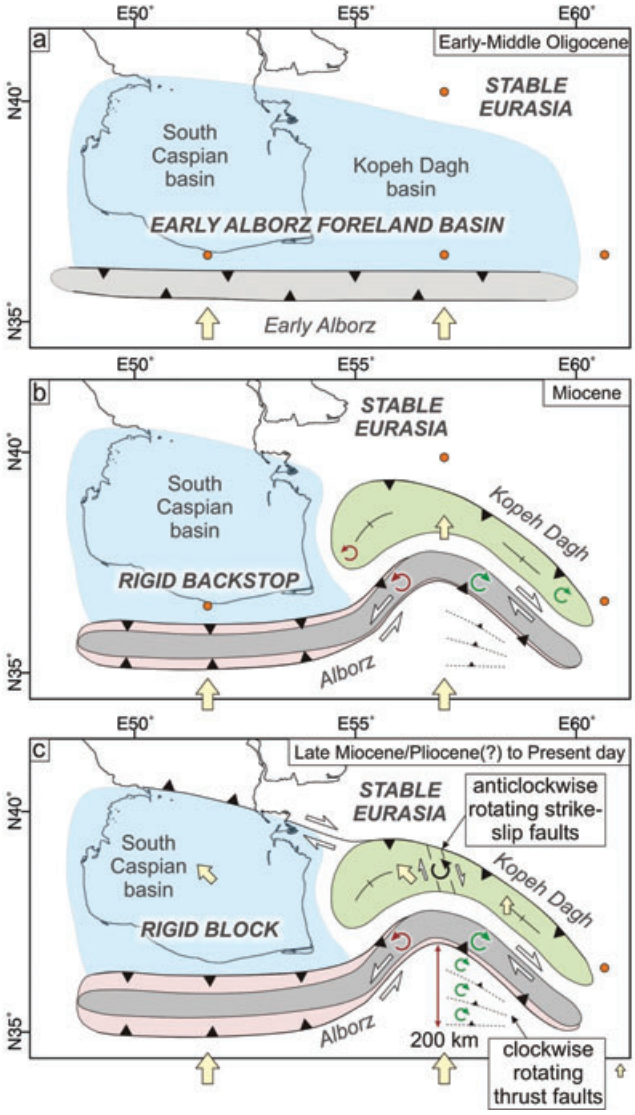

Figure 26. (a) Simplified reconstruction of the tectonics of North Iran in the Early-Middle Oligocene, before uplift of the Kopeh Dagh foreland basin. At this time the recently uplifted Alborz mountains probably formed a linear range, striking E–W across the region, south of the South Caspian-Kopeh Dagh basin to the north. Yellow arrows show schematically the northward direction of shortening, and the orange circles represent non-deforming Eurasia. (b) Uplift of the Kopeh Dagh basin to form the Kopeh Dagh mountains, coupled with continued shortening in the West and Central Alborz, south of the rigid South Caspian backstop, resulted in the northward deflection of the East Alborz in NE Iran. The onset of strike slip faulting in the East Alborz (left-lateral west of 57°E, right-lateral east of 57°E) was probably contemporaneous with deflection of the range. (c) Eventually shortening across the W Kopeh Dagh mountains began to be accommodated by the westward extrusion of the West Kopeh Dagh-South Caspian block, and the northward subduction of the South Caspian beneath the North Caspian.

Revised plate-closure models of McQuarrie *et al.* (2003) indicate the rate of Arabia–Eurasia convergence has been almost constant at 20–24 mm yr^{-1} over the last 20 Ma. Assuming the present-day GPS velocities across Central Iran have also been constant over the late Cenozoic, 200 ± 20 km of N–S shortening would be

accumulated in 30 ± 8 Ma, based on a northward shortening rate of 6–8 mm yr^{-1} at 57°E. This age is consistent with the the geological estimate for the onset of uplift in the Kopeh Dagh (post 30 Ma) (e.g. Allen & Armstrong 2008, see also Section 2.2). Nevertheless, a number of major tectonic events have affected north Iran during this period, such as rapid exhumation of the West Alborz at 12 Ma (Guest *et al.* 2006a), increased subsidence in the NW South Caspian basin at 5.5 Ma (Allen *et al.* 2002), and a possible kinematic change in the Central Alborz at 1.8 Ma (Ritz *et al.* 2006). Therefore, it cannot be assumed that the accommodation of 6–8 mm yr^{-1} N–S shortening across NE Iran has been constant over this period. Nevertheless, the East Alborz mountains probably played a more important role in accommodating Arabia–Eurasia shortening prior to the formation of the Kopeh Dagh, and the onset of South Caspian subduction beneath Eurasia (both 12 Ma or younger). The Sabzevar and Kuh-e-Sorkh mountain ranges both lie south of the deflected East Alborz range, and yet also accommodate N–S shortening. Therefore, the total N–S shortening across NE Iran, north of the Doruneh fault, since the start of Arabia–Eurasia collision at ∼30 Ma must exceed 200 ± 20 km.

9 CONCLUSIONS

The most important result of this work has been the identification of major active thrust faults bounding the south side of the East Alborz (east of 57°E) and Sabzevar mountains, and the north side of the Kuh-e-Sorkh mountains in NE Iran, which are responsible for major historical earthquakes in the region. The contribution of these faults to regional shortening is small (each range accommodates 1–2 mm yr^{-1}), with the remainder being accommodated across the Kopeh Dagh mountains, which form the northern limit of deformation in NE Iran. Future, more comprehensive Quaternary dating and GPS investigations coupled with focused studies looking at both the surface and subsurface structure and palaeomagnetic evolution of the region are essential for testing and further refining our kinematic model.

Total shortening across the East Alborz and Kopeh Dagh mountains since uplift of the Kopeh Dagh basin may be 200 ± 20 km, based on the topographic deflection of the East Alborz range, which at present-day rates of shortening would be accommodated in ∼30 Ma, and is in agreement with geological estimates for the onset of uplift in the Kopeh Dagh in the early-to-middle Oligocene.

ACKNOWLEDGMENTS

We thank the Geological Survey of Iran for organizing all aspects of the fieldwork, and for their continued support of our work in Iran. Reza Tajik and Asghar Dolati provided valuable support both in the field and measuring GPS profiles at Neyshabur and Sabzevar. We are particularly grateful to Mr Taheri, Nasser Naimi and Nassir Nadheri, who helped organize various aspects of the fieldwork, and for making JH, RW and JJ so welcome at GSI Mashad. This work benefited from useful discussion with Dr M. Ghorashi, Jeff Ritz, Nicky White, Mahnaz Rezaeian, Dan McKenzie, Keith Priestley, Barry Parsons, Bob Engdahl, Eric Bergman, Jean-Philippe Avouac, Daniel Rham, Brian Emmerson and Beth Shaw. JH would like to thank the Centre for the Observation and Modelling of Earthquakes and Tectonics (COMET) for financial assistance, and for providing a stimulating environment for the discussion of active tectonics. Various images in this paper were created using the public domain Generic Mapping Tools (GMT) software (Wessel & Smith 1998). Ikonos and Quickbird satellite images were obtained from Google Earth (©2010 Google, ©2010 GeoEye, ©2010 DigitalGlobe), Landsat7 images from the USGS and NASA, via the Global Land Cover Facility at the University of Maryland, and ASTER and SRTM were obtained from the USGS and NASA. This work benefited greatly from careful reviews by Mike Taylor and three anonymous reviewers.

REFERENCES

Afshar-Harb, A., 1979. The stratigraphy, tectonics and petroleum geology of the Kopet Dagh region, northern Iran, *PhD thesis*, Imperial College of Science and Technology, London.

Alavi, M., 1992. Thrust tectonics of the Binalood region, NE Iran, *Tectonics,* **11**(2), 360–370.

Alavi, M., 1996. Tectonostratigraphic synthesis and structural style of the Alborz mountain system in northern Iran, *J. Geodyn.,* **21**(1), 1–33.

Allen, M. & Armstrong, H., 2008. Arabia-Eurasia collision and the forcing of mid-Cenozoic global cooling, *Palaeogeogr., Palaeoclimatol., Palaeoecol.,* **265,** 52–58.

Allen, M., Jones, S., Ismail-Zadeh, A., Simmons, M. & Anderson, L., 2002. Onset of subduction as the cause of rapid Pliocene-Quaternary subsidence in the South Caspian Basin, *Geology,* **30,** 775–778.

Allen, M., Vincent, S., Alsop, G., Ismail-zadeh, A. & Flecker, R., 2003. Late Cenozoic deformation in the South Caspian region: effects of a rigid basement block within a collision zone, *Tectonophysics,* **366,** 223–239.

Allen, M., Walker, R., Jackson, J., Blanc, E.-P., Talebian, M. & Ghassemi, M., 2006. Contrasting styles of convergence in the Arabia-Eurasia collision: Why escape tectonics does not occur in Iran, in *Postcollisional Tectonics and Magmatism in the Mediterranean Region and Asia,* GSA Special Paper Vol. 409, pp. 579–589, eds Dilek, Y. & Pavlides, S., Geological Society of America, Boulder, CO.

Ambraseys, N. & Bilham, R., 2003. Earthquakes in Afghanistan, *Seismol. Res. Lett.,* **74,** 107–123.

Ambraseys, N. & Melville, C., 1982. *A History of Persian Earthquakes,* Cambridge University Press, Cambridge.

Axen, G.J., Lam, P.S., Grove, M., Stockli, D.F. & Hassanzadeh, J., 2001. Exhumation of the west-central Alborz Mountains, Iran, Caspian subsidence, and collision-related tectonics, *Geology,* **29**(6), 559–562.

Baker, C., 1993. Active seismicity and tectonics of Iran, *PhD thesis*, University of Cambridge.

Berberian, M., 1981. Active faulting and tectonics of Iran, in *Zagros-Hindu Kush-Himalaya Geodynamic Evolution,* Geodynamic Series, chapter 3, pp. 33–69, eds Gupta, H., Delany, F., American Geophysical Union.

Berberian, M. & King, G., 1981. Towards a paleogeography and tectonic evolution of Iran, *Can. J. Earth Sci.,* **18**(2), 210–265, Exhaustive geological history of Iran.

Berberian, M. & Yeats, R., 1999. Patterns of Historical Earthquake Rupture in the Iranian Plateau, *Bull. seism. Soc. Am.,* **89,** 120–139.

Berberian, M. *et al.*, 2001. The 14 March 1998 Fandoqa earthquake (Mw 6.6) in Kerman province, S.E. iran: re-rupture of the 1981 Sirch earthquake fault, triggering of slip on adjacent thrusts, and the active tectonics of the Gowk fault zone., *Geophys. J. Int.,* **146,** 371–398.

Boyer, S. & Elliott, D., 1982. Thrust systems, *Am. Assoc. Petrol. Geol. Bull.,* **66**(9), 1196–1230.

Copley, A. & Jackson, J., 2006. Active tectonics of the Turkish-Iranian Plateau, *Tectonics,* **25**(TC6006), 1–19.

Daëron, M., Avouac, J.-P. & Charreau, J., 2007. Modeling the shortening history of a fault-tip fold using structural and geomorphic records of deformation, *J. geophys. Res.,* **112,** B03S13.

Devlin, W., Cogswell, J., Gaskins, G., Isaksen, G., Pitcher, D., Puls, D., Stanley, K. & Wall, G., 1999. South Caspian Basin: young, cool, and full of promise, *GSA Today,* **9**(7), 1–9.

Doebrich, J. & Wahl, R., 2006. Geologic and Mineral Resource Map of Afghanistan, *USGS Open-File Report 2006–1038,* p. http://pubs.usgs.gov/of/2006/1038/.

Engdahl, E., van der Hilst, R. & Buland, R., 1998. Global teleseismic earthquake relocation with improved travel times and procedures for depth determination, *Bull. seism. Soc. Am.,* **88**(3), 722–743.

Engdahl, E., Jackson, J., Myers, S., Bergman, E. & Priestley, K., 2006. Relocation and assessment of seismicity in the Iran region, *Geophys. J. Int.,* **167,** 761–788.

Fattahi, M. & Walker, R., 2007. Luminescence dating of the last earthquake of the Sabzevar thrust fault, NE Iran, *Quarter. Geochronol.,* **2,** 284–289.

Fattahi, M., Walker, R., Hollingsworth, J., Bahroudi, A., Nazari, H., Talebian, M., Armitage, S. & Stokes, S., 2006. Holocene slip-rate on the Sabzevar thrust fault, NE Iran, determined using optically stimulated luminescence (OSL), *Earth planet. Sci. Lett.,* **245**(3–4), 673–684.

Fattahi, M., Walker, R., Khatib, M., Dolati, A. & Bahroudi, A., 2007. Slip-rate estimate and past earthquakes on the Doruneh fault, eastern Iran, *Geophys. J. Int.,* **168,** 691–709.

Golonka, J., 2004. Plate tectonic evolution of the southern margin of Eurasia in the Mesozoic and Cenozoic, *Tectonophysics,* **381,** 235–273.

Guest, B., Axen, G., Lam, P. & Hassanzadeh, J., 2006a. Late Cenozoic shortening in the west-central Alborz Mountains, northern Iran, by combined conjugate strike-slip and thin-skinned deformation, *Geosphere,* **2**(1), 35–52.

Guest, B., Stockli, D., Grove, M., Axen, G., Lam, P. & Hassanzadeh, J., 2006b. Thermal histories from the central Alborz Mountains, northern Iran: implications for the spatial and temporal distribution of deformation in northern Iran, *Geol. Soc. Am. Bull.,* **118,** 1507–1521.

Hempton, M., 1987. Constraints on Arabian plate motion and extension history of the Red Sea, *Tectonics,* **6,** 687–705.

Hessami, K., Nilforoushan, F. & Talbot, C., 2006. Active deformation within the Zagros Mountains deduced from GPS measurements, *J. Geol. Soc.,* **163**(1), 143–148.

Hilley, G., Blisniuk, P. & Strecker, M., 2005. Mechanics and erosion of basement-cored uplift provinces, *J. geophys. Res.,* **110,** B12409, doi:10.1029/2005JB003704.

Hollingsworth, J., Jackson, J., Walker, R., Gheitanchi, M. & Bolourchi, M., 2006. Strike-slip faulting, rotation, and along-strike elongation in the Kopeh Dagh mountains, NE Iran, *Geophys. J. Int.,* **166,** 1161–1177.

Hollingsworth, J., Jackson, J., Walker, R. & Nazari, H., 2008. Extrusion tectonics and subduction in the eastern South Caspian region since 10 Ma, *Geology,* **36**(10), 763–766.

Hollingsworth, J., Jackson, J., Walker, R. & Nazari, H., 2009. Extrusion tectonics and subduction in the eastern South Caspian region since 10 Ma: reply, *Geology,* doi:10.1130/G30529Y.1, e199–e200.

Huber, H., 1977a. Geological map of Iran – Sheet No. 2 – NE Iran, *NIOC*.

Huber, H., 1977b. Geological map of Iran – Sheet No. 3 – NE Iran, *NIOC*.

Jackson, J., 2006. Fatal attraction: living with earthquakes, the growth of villages into megacities, and earthquake vulnerability in the developing world, *Phil. Trans. R. Soc. A,* **364,** 1911–1925.

Jackson, J. & McKenzie, D., 1984. Active tectonics of the Alpine-Himalayan Belt between western Turkey and Pakistan, *Geophys. J. R. astr. Soc.,* **77**(1), 185–264.

Jackson, J. & McKenzie, D., 1988. The relationship between plate motions and seismic moment tensors, and the rates of active deformation in the Mediterranean and Middle East, *Geophys. J.,* **93,** 45–73.

Jackson, J., Haines, J. & Holt, W., 1995. The accommodation of Arabia–Eurasia plate convergence in Iran, *J. geophys. Res.,* **100**(B8), 15 205–15 219.

Jackson, J., Priestley, K., Allen, M. & Berberian, M., 2002. Active tectonics of the South Caspian Basin, *Geophys. J. Int.,* **148,** 214–245.

King, G., Stein, R. & Rundle, J., 1988. The growth of geological structures by repeated earthquakes, 1: conceptual framework, *J. geophys. Res.,* **93,** 13 307–13 318.

Krumsiek, K., 1976. Zur Bewegung der Iranisch-Afghanischen Platte, *Geologische Rundschau,* **65,** 909–929.

Lyberis, N. & Manby, G., 1999. Oblique to orthogonal convergence across the Turan block in the post-Miocene, *Am. Assoc. Petrol. Geol. Bull.,* **83**(7), 1135–1160.

Maggi, M., Jackson, J., McKenzie, D. & Priestley, K., 2000. Earthquake focal depths, effective elastic thickness, and the strength of the continental lithosphere, *Geology,* **28**(6), 495–498.

Masson, F., Chery, J., Hatzfeld, D., Martinod, J., Vernant, P., Tavakoli, F. & Ghafory-Ashtiani, M., 2005. Seismic versus aseismic deformation in Iran inferred from earthquakes and geodetic data, *Geophys. J. Int.,* **160**(1), 217–226.

Masson, F., Anvari, M., Djamour, Y., Walpersdorf, A., Tavakoli, F., Daignières, M., Nankali, H. & van Gorp, S., 2007. Large-scale velocity field and strain tensor in Iran inferred from GPS measurements: new insight for the present-day deformation pattern within NE Iran, *Geophys. J. Int.,* **170,** 436–440.

McClusky, S., Reilinger, R., Mahmoud, S., Ben Sari, D. & Tealeb, A., 2003. GPS constraints on Africa (Nubia) and Arabia plate motions, *Geophys. J. Int.,* **155**(1), 126–138.

McKenzie, D., 1972. Active tectonics of the Mediterranean region, *Geophys. J. R. astr. Soc.,* **30,** 109–185.

McQuarrie, N., Stock, J., Verdel, C. & Wernicke, B., 2003. Cenozoic evolution of Neotethys and implications for the causes of plate motions, *Geophys. Res. Lett.,* **30**(20).

Meyer, B., Mouthereau, F., Lacombe, O. & Agard, P., 2006. Evidence of quaternary activity along the deshir fault: implication for the tertiary tectonics of central iran, *Geophys. J. Int.,* **164,** 192–201.

Molnar, P. & Tapponnier, P., 1975. Cenozoic tectonics of Asia: effects of a continental collision, *Science,* **189,** 419–426.

Natal'in, B.A. & Şengör, A., 2005. Late Palaeozoic to Triassic evolution of the Turan and Scythian platforms: the pre-history of the Palaeo-Tethyan closure, *Tectonophysics,* **404**(3-4), 175–202.

Nissen, E. *et al.*, 2009. The late Quaternary slip-rate of the Har-Us-Nuur fault (Mongolian Altai) from cosmogenic î0Be and luminescence dating, *Earth planet. Sci. Lett.,* (**286**(3–4), 467–478.

Regard, V. *et al.*, 2005. Cumulative right-lateral fault slip rate across the Zagros-Makran transfer zone: role of the Minab-Zendan fault system in accommodating Arabia-Eurasia convergence in southeast Iran, *Geophys. J. Int.,* **162**(1), 177–203.

Reilinger, R. *et al.*, 2006. GPS constraints on continental deformation in the Africa-Arabia-Eurasia continental collision zone and implications for the dynamics of plate interactions, *J. geophys. Res.,* **111,** B05411.

Rezaeian, M., 2008. Active seismicity and tectonics of Iran, *PhD thesis,* Univ. Cambridge.

Rezanov, I., 1959. *Tectonics and Seismicity in the Turkmeno-Horasan Mountains,* Academy of Sciences, USSR, Moscow.

Ritz, J.-F., Nazari, H., Ghassemi, A., Salamati, R., Shafei, A., Solaymani, S. & Vernant, P., 2006. Active transtension inside central Alborz: a new insight into northern Iran–Southern Caspian geodynamics, *Geology,* **34**(6), 477–480.

Ruleman, C., Crone, A., Machette, M., Haller, K. & Rukstales, K., 2007. Map and database of probable and possible Quaternary faults in Afghanistan, U.S. Geological Survey Open-File Report 2007-1103.

Ruttner, A.W., 1993. Southern borderland of Triassic Laurasia in NE Iran, *Geologische Rundschau,* **82,** 110–120.

Sella, G.F., Dixon, T.H. & Mao, A., 2002. Revel: a model for Recent plate velocities from space geodesy, *J. geophys. Res.,* **107**(B4), doi:10.1029/2000JB000033.

Şengör, A., 1984. The Cimmeride Orogenic System and the Tectonics of Eurasia, *Geol. Soc. Am. Special Paper,* **195,** 1–82.

Şengör, A., 1987. Tectonics of the tethysides: Orogenic collage development in a collisional setting, *Ann. Rev. Earth planet. Sci.,* **15,** 213–244.

Shabanian, E., Bellier, O., Siame, L., Arnaud, N., Abbassi, M. & Cochemé, J., 2009a. New tectonic configuration in NE Iran: active strike-slip faulting between the Kopeh Dagh and Binalud mountains, *Tectonics,* **28,** TC5002.

Shabanian, E., Siame, L., Bellier, O., Benedetti, L. & Abbassi, M., 2009b. Quaternary slip rates along the northeast boundary of the Arabia-Eurasia collision zone (Kopeh Dagh Mountains, north-east Iran), *Geophys. J. Int.,* **178,** 1055–1077.

Stein, R., King, G. & Rundle, J., 1988. The growth of geological structures by repeated earthquakes, 2: field examples of continental dip-slip faults, *J. geohys. Res.,* **93,** 13 319–13 331.

Stöcklin, J., 1968. Structural history and tectonics of Iran: a review, *Am. Assoc. Petrol. Geol. Bull.,* **52**(7), 1229–1258.

Stöcklin, J., 1974. Possible ancient continental margins in Iran, in *Geology of Continental Margins,* pp. 873–877, eds Burke, C. & Drake, C., Springer-Verlag, New York.

Talebian, M. & Jackson, J., 2004. A reappraisal of earthquake focal mechanisms and active shortening in the Zagros mountains of Iran, *Geophys. J. Int.,* **156**(3), 506–526.

Talebian, M. *et al.*, 2006. The Dahuiyeh (Zarand) earthquake of 2005 February 22 in central Iran: reactivation of an intramountain reverse fault, *Geophys. J. Int.,* **164**(1), 137–148.

Tapponnier, P. & Molnar, P., 1976. Slip-line field theory and large-scale continental tectonics, *Nature,* **264,** 319–324.

Tapponnier, P., Mattauer, M., Proust, F. & Cassaigneau, C., 1981. Mesozoic ophiolites, sutures and large scale tectonic movements in Afghanistan, *Earth planet. Sci. Lett.,* **52,** 355–371.

Tatar, M., Hatzfeld, D., Martinod, J., Walpersdorf, A., Ghafori-Ashtiany, M. & Chéry, J., 2002. The present-day deformation of the central Zagros from GPS measurements, *Geophys. Res. Lett.,* **29**(19), doi:10.1029/2002GL015427.

Tatavousian, S., Zohreh-Bakhsh, A., Sahandi, M., Hoseyni, M., Pour, H., Tehrani, A., S., S. & Tabar, F., 1993. Geological quadrangle map of Iran No. J4 (Sabzevar sheet), scale 1:250 000, Geological Survey Of Iran.

Tchalenko, J.S., 1975. Seismicity and structure of the Kopet Dagh (Iran, USSR), *Phil. Trans. R. Soc. Lond., A.,* **278**(1275), 1–28.

Treloar, P. & Izatt, C., 1993. Tectonics of the Himalayan collision between the Indian Plate and the Afghan Block: a synthesis, *Geol. Soc., Lond.,* Special Publications, **74,** 69–87.

Vernant, P. *et al.*, 2004a. Deciphering oblique shortening of central Alborz in Iran using geodetic data, *Earth planet. Sci. Lett.,* **223,** 177–185.

Vernant, P. *et al.*, 2004b. Present-day crustal deformation and plate kinematics in the Middle East constrained by GPS measurements in Iran and northern Oman, *Geophys. J. Int.,* **157**(1), 381–398.

Vincent, S., Allen, M., Ismail-Zadeh, A., Flecker, R., Foland, K. & Simmons, M., 2005. Insights from the Talysh of Azerbaijan into the Paleogene evolution of the South Caspian region, *Geol. Soc. Am. Bull.,* **117,** 1513–1533.

Walker, R. & Jackson, J., 2002. Offset and evolution of the Gowk fault, SE Iran: a major intra-continental strike-slip system, *J. Struct. Geol.,* **24,** 1677–1698.

Walker, R. & Jackson, J., 2004. Active tectonics and late Cenozoic strain distribution in central and eastern Iran, *Tectonics,* **23,** TC5010, doi:10.1029/2003TC001529.

Walker, R., Jackson, J. & Baker, C., 2003. Surface expression of thrust faulting in eastern Iran: source parameters and surface deformation of the 1978 Tabas and 1968 Ferdows earthquake sequences, *Geophys. J. Int.,* **152,** 749–765.

Walpersdorf, A. *et al.*, 2006. Difference in the GPS deformation pattern of north and central zagros (Iran), *Geophys. J. Int.,* **167**(3), 1077–1088.

Wellman, H.W., 1966. Active wrench faults of Iran, Afghanistan, and Pakistan, *Geologische Rundschau,* **55,** 716–735.

Wessel, P. & Smith, W.H.F., 1998. New, improved version of Generic Mapping Tools released, *EOS, Trans. Am. Geophys. Un.,* **79**(47), 579.

Zanchi, A., Berra, F., Mattei, M., Ghassemi, M. & Sabouri, J., 2006. Inversion tectonics in central Alborz, Iran, *J. Struct. Geol.,* **28,** 2023–2037.

SUPPORTING INFORMATION

Additional Supporting Information may be found in the online version of this article:

Appendix S1. This appendix contains a summary geological map showing the major units in the NE Iran region (PDF format).
Appendix S2. This appendix describes the methodology behind optically stimulated luminescence dating (PDF format).
Appendix S3. This appendix outlines the different ways of calculating horizontal shortening rate across a thrust fault according to differences in the subsurface geometry of the fault (PDF format).
Appendix S4. This appendix gives the results of an elastic dislocation model, which is used to reproduce the topography created by slip on the Neyshabur fault. The model is used to better constrain the subsurface geometry of the fault, which dips to the north by 50–80°, and extends from 1 km to 0.5 km depth beneath the surface. These results suggest slip occurs on a blind thrust ramp which splays out from the North Neyshabur fault (PDF format).

Please note: Wiley-Blackwell are not responsible for the content or functionality of any supporting materials supplied by the authors. Any queries (other than missing material) should be directed to the corresponding author for the article.